CHALMERS
UNIVERSITY OF TECHNOLOGY

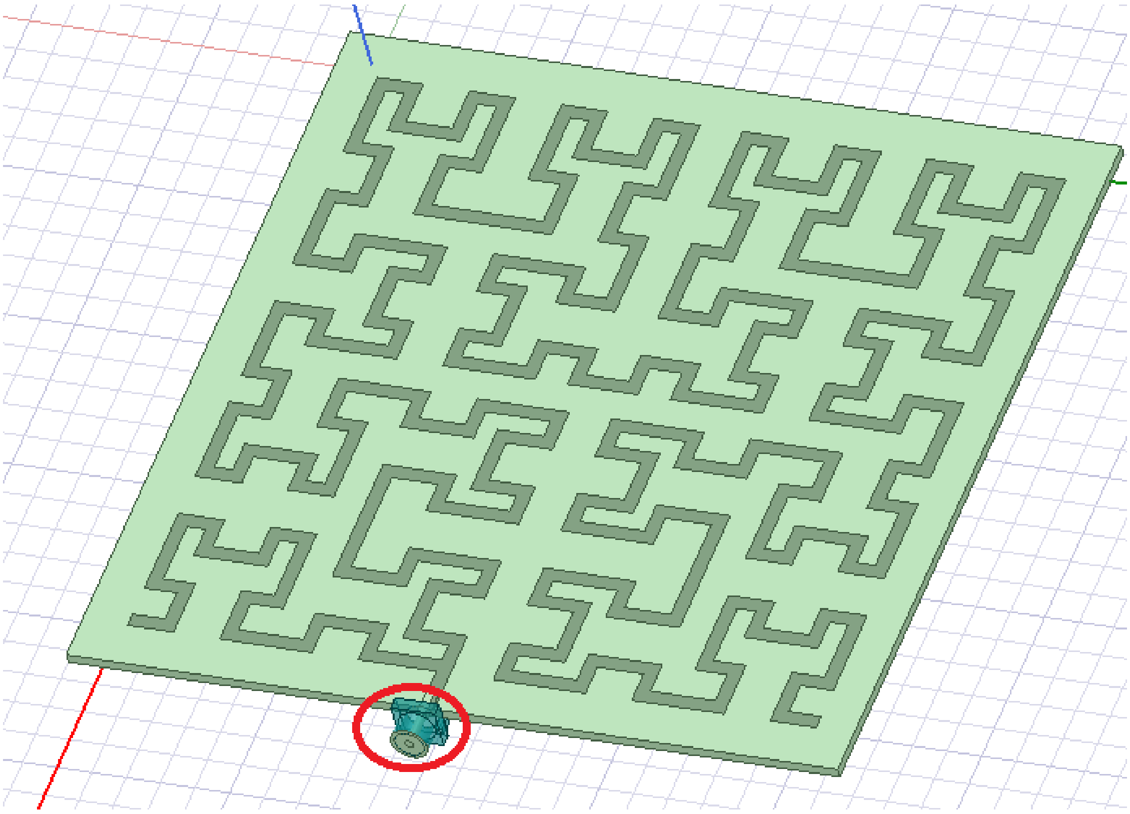

Sensitivity Verification for Hilbert Antenna in UHF PD Measurements

Master's Thesis Wireless, Photonics and Space Engineering

Abdalmonam Zahed

Department of Electrical Engineering
Chalmers University of Technology
Gothenburg, Sweden 2019

Master's thesis 2019

Sensitivity Verification for Hilbert Antenna in UHF PD Measurements

Abdalmonam Zahed

Department of Electrical Engineering
Chalmers University of Technology
Gothenburg, Sweden 2019

Sensitivity Verification for Hilbert Antenna in UHF PD Measurements
Abdalmonam Zahed

Supervisor: Mohammad Kharezy, Electrical Engineering / RISE Research Institute of Sweden
Examiner: Yuriy Serdyuk, Department of Electrical Engineering

Master's Thesis 2019
Department of Electrical Engineering

Chalmers University of Technology
SE-412 96 Gothenburg
Telephone +46 31 772 1000

Cover: Simulated 4^th order Hilbert fractal antenna with the feeding point indicated by the circle, done in HFSS.

Typeset in LaTeX
Gothenburg, Sweden 2019

Sensitivity Verification for Hilbert Antenna in UHF PD Measurements

Abdalmonam Zahed
Department of Electrical Engineering
Chalmers University of Technology

Abstract

In high voltage transmission and distribution networks, transformers are considered as one of the most important assets. After a transformer exceeds its life expectancy, it is most likely taken out of service. This results in huge costs, which can be mitigated if certain indicators implying insulation failure is monitored. One of such indicator is the level of partial discharges (PD), which is usually measured when a transformer is offline.

In this thesis, a study of the applicability of a wide-band antenna for partial discharge detection was performed. A comprehensive analysis of the Hilbert fractal antenna response was conducted under different environmental settings and compared to the simulated response. Furthermore, sensitivity of the antenna was analyzed experimentally utilizing three different types of sources of partial discharges, namely: a sharp point against metallic plane, a void in solid dielectric material and twisted pair. The three sources were tested in air and inside an oil-filled tank. To identify the sensitivity of the antenna, the responses were recorded, the energy of the received signals were evaluated and correlated with the apparent PD charge measured by a conventional tool. The tests showed weak positive correlation in case of air. It became more pronounced when partial discharges source and sensing antenna were immersed in transformer oil. The study confirmed that Hilbert fractal antenna can be utilized for detection and monitoring of partial discharges in liquid high voltage insulation systems.

Keywords: Hilbert antenna, ultra-high frequency, sensitivity, partial discharge, liquid insulation, correlation analysis.

Acknowledgements

This project has been performed with the support from RISE Research Institutes of Sweden. In order to give thanks where it is due, this section is dedicated to those whom without their help this project would not have been completed. First and foremost, I would like to give my sincerest thanks and appreciation to my examiner Yuriy Serdyuk and advisor Mohammad Kharezy, who guided me throughout the thesis project and provided support where needed. The time and effort they spent helping me and providing the resources I needed to complete my project played an important role in allowing me to finish on time. Special thanks to Espen Doedens who was always available in the lab to give a hand when needed. My trips to RISE Research Institutes of Sweden also benefited me during the course of this project, where Claes Wingqvist was always there to provide support for practical testing of the sensor in the microwave lab. This section would not be complete without thanking the person who spent her time reading through this report helping me improve the writing style and motivating me to finish it, the amazing Inga Sierpińska. Furthermore, the support I had, have and will still gain from my family back home was the light I needed to guide my academic carrier and push me to become a better person. Finally, the family I gained here in Sweden had me believe that kinship is not what makes strong bonds, but caring, cherishing and supporting friends are what we will always keep in our memories forever and ever. Thus, the biggest thanks would go to Katrin Siess, Rasika Somalwar and Issam Maarouf, may we always be connected through time and space.

Abdalmonam Zahed, Gothenburg, May 2019

Contents

List of Figures

List of Tables

1

Introduction

Almost all high voltage generation and distribution systems contain expensive and essential assets. Some of these equipment have a limited life span with an approximate life expectancy that indicates when a component must be taken out of service. However, life expectancy as many other estimated specifications is just a prediction of the material's durability levels and not an exact measure. Therefore, as HV transformers near the end of their life expectancy, they are usually taken out of service, which costs governments and authorities a significant amount of time and money. This is a very costly and time consuming operation, not to mention that it would result in a blackout in some sections of the grid unless measures were taken in advance. To save some money and add few more years to the life of such HV devices, monitoring of these devices is essential, where certain indicators can be observed which would assist in evaluating the condition of the HV device. Many indications can be monitored and investigated before deciding whether a device is no longer capable of performing at the standard quality. To investigate the status of a device and increase the life span of such components, **condition based maintenance** (CBM) is applied. CBM can be defined as a strategy of monitoring the actual status of a resource to determine which maintenance method must be used. By maintaining the system or component, for example an oil-filled transformer, one can decide with high certainty whether the device is fully operational, requires maintenance or has to be taken out of service. Thus, to reach this level of confidence in the apparatus used for CBM, an study of the sensitivity of the sensor and detection system has to be implemented with respect to a known standardized partial discharge measuring device [8]. Current detection systems require the use of matched circuits and coupling capacitors, these systems can tell the amount of charges released by a partial discharge (PD) phenomena but does not capture the actual PD signal. Digitizing the original PD signal allows users to have more options when monitoring such an indicator, as PD can be harmful to the HV insulation and are considered as a main indication of insulation failure.

1.1 Purpose

The purpose of this thesis work is to investigate performance of the 4^{th} order Hilbert micro-strip antenna with respect to PD acquisition and measurements. The sensor will be used to detect UHF PD signal that contain an ultra-wide band of frequencies. To cover the ultra-wide band, this sensor is chosen based on the fact that it can be designed to cover a wide band ranging from $300MHz$ to $3GHz$. Being able to detect frequencies within the aforementioned range implies that the Hilbert fractal antenna (HFA) would be able to collect many frequency components belonging to the PD impulse. The same antenna would be used in PD monitoring and its captured energy level must be calibrated in order to measure its sensitivity to the PD phenomena.

1.2 Motivation

Current literature shows many ways of detecting the partial discharge phenomena, where each source states that their sensor is reliable with high sensitivity to certain PD types under specified conditions [10]. Since sensors across the literature operate by detecting different emissions types of PD, it was shown that sensors that utilize the same type of emission have a varying operational bandwidth or sensitivity. For example, antennas used to detection the EM emissions generated from PD sources, have different sensitivity and shows varying results when different antenna designs are used to monitor the same PD source. Providing a procedure to measure the sensitivity of a sensor with respect to a typical and common PD measurement device is essential to compare results across different experimental setups with a known reference such as the IEC 60270 PD apparent charge meter.

1.3 Objectives

A study of the sensitivity of the sensor in order to establish a plane of reference for the HFA when used in PD measurements. In addition, a comprehensive analysis of the Hilbert antenna must be investigated to identify the following parameters:

- S_{11} parameter (reflection coefficient of the antenna showing operational bandwidth of the sensor)
- Radiation pattern
- Operational bandwidth
- Sensitivity to PD occurrences
- Effects of different propagation media on the antenna response

1.4 Sustainability and Ethical Issues

Power transformers have essential parts that are not replaceable, such as the core winding and the paper insulation. These parts and other parts of the transformer are made of materials produced specifically for the use of power transformers. Power transformers weigh several tons and they take a very large space. Thus, when replacing and old power transformer a tremendous amount of energy and resources are required. Another issue arises with old discarded power transformer which is whether is it possible to recycle the materials in an environmentally friendly way that would leave the least amount of impact on the environment.
Thus, the analysis and monitoring of the partial discharge phenomena, specifically using the UHF detection method can aid in a prolonged operational life time of the power transformer, which means a more efficient and sustainable way of utilizing current resources.

2

Literature Review

2.1 Partial Discharge

Partial discharge is the most common indicator of insulation failure in high voltage systems. PD occurs when a high voltage system is subjected to highly concentrated electrical stress for prolonged periods during operation. According to IEC 60270 a partial discharge is a localized breakdown of small part of an insulating material, whether it is solid or liquid, under HV stress [11]. The PD phenomena produces different types of emissions in the form of visible, radio and acoustic waves, each type can be detected in a different way. The defect type, size and geometry of the material causing the partial discharge can help in identifying what type of PD would be generated, by investigating the captured signal from the PD emission and running it through a smart classification system [10]. PD can also play a role in accelerating the aging of HV devices by reducing the device‘s life span [16]. To further illustrate, the following sections explain in details several PD types and their sources.

2.1.1 Types of Partial Discharge Sources

The partial discharge phenomena can be induced by various sources and processes within a HV transformer. The geometry, location, intensity and shape of PD signals depend on multiple variables [9]. A few selected types of partial discharge will be discussed in this section in detail and how to simulate them in laboratory environments.

2.1.1.1 Twisted Pair PD source

A twisted pair PD source is used to simulate defects that appear inside motor windings insulation. The twisted pair PD source is usually made of simple wires twisted with each other with a specific length for each twist. The number of twists along with the type of material used play an important role in determining the generated PD intensity and its rate of occurrence. The intensity of this PD type can be controlled by changing the magnitude of the applied voltage. Figure 2.1 shows a sample of a twisted pair source that can be used to generate this PD.

Figure 2.1: Twisted pair PD source.

2.1.1.2 Sharp Point PD source

Partial discharge usually develops due to a sharp conductive protrusion within the insulated HV unit. This sharp protrusion can be a result of some form of mechanical distortion within the transformer tank, where electric field intensifies at the tip of the sharp point to the limit where it reaches insulation breakdown. This causes the partial discharge phenomena to occur. The sharp point PD can have a fixed location within the transformer tank or it can be generated by a particle moving throughout the insulating medium. Also, its presence within the HV unit can be very harmful to the insulation as it can aggravate the manifestation of PD, which would damage the device [9]. Figure 2.2 below shows a sharp point electrode (up) and a flat plate (down). The sharp point electrode would be connected to a high voltage source, whereas the lower flat plate would be grounded. Having the flat conducting plate at lower potential creates a path for the electrons to travel from an intensified higher electric field at the tip of the sharp conducting point towards a lower potential, which is the flat plate, connected to ground. The distance between both electrodes determines how much potential difference is needed to generate partial discharge. Certainly, the medium, the geometry of the sharp point, the material and the shape of the signal applied contribute to changes in generating this PD type.

Figure 2.2: Sharp point PD source.

2.1.1.3 Void PD source

This type of PD can be generated by air bubbles within liquid insulation or cracks in the solid insulation of a HV device. Several parameters influence the type of the void PD, such as the gas within the void, pressure of the gas, void shape and volume [16]. Void PD is generated by air bubbles within liquid dielectrics usually pop after the PD is generated, whereas void PD generated within cracks in solid insulation can be an indication of direct insulation breakdown as well as **"accelerated aging process"** [16]. Figure 2.3 shows how to simulate a void PD simply by fusing three plastic discs together, where the middle disc has a circular cut at its center, effectively trapping air in the contained area. On the top is an electrode connected to a HV source, and the bottom is a grounded electrode. Placing this apparatus within an oil-filled tank can generate signals that simulates an actual bubble void PD in oil-filled transformers.

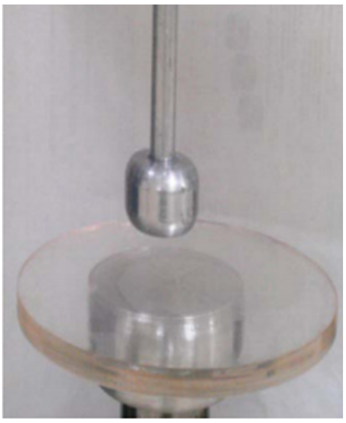

Figure 2.3: Void point PD source.

2.2 Methods of Detecting Partial Discharge

Several physical phenomena are generated by the partial discharge activity, such as: heat, chemical effects, optical light, pressure waves, electromagnetic radiation and other electrical signs. Figure 2.4 shows the different physical manifestations of a PD occurrence within a HV system. There are many ways to detect partial discharge, the following sections contain a detailed explanation of each method: the advantages and disadvantage of each method and what type of sensors or traces can be used.

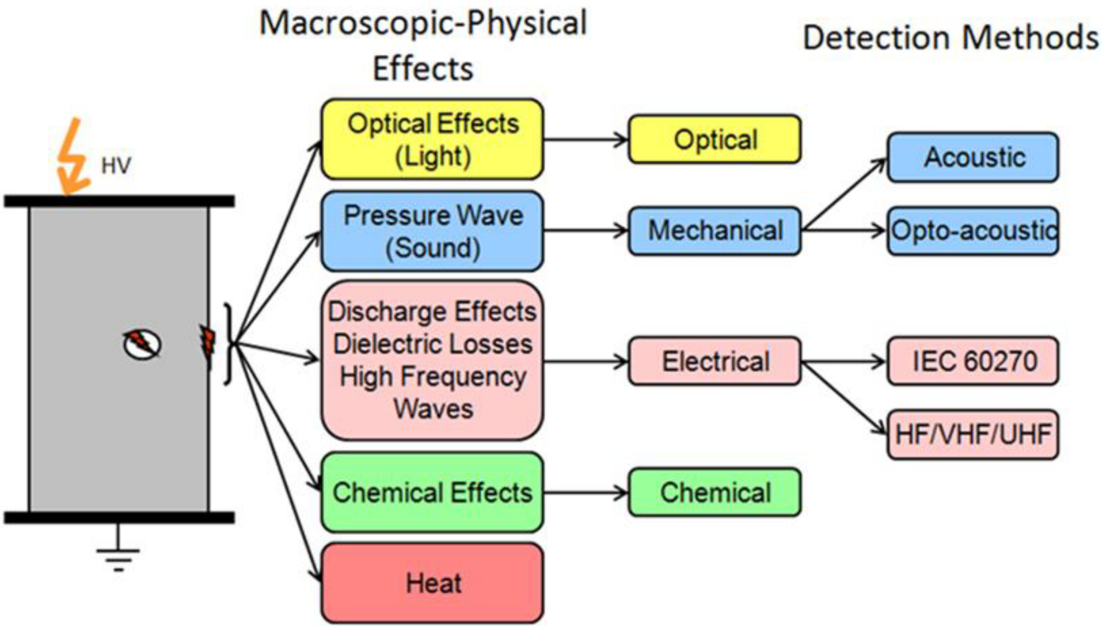

Figure 2.4: Different physical signs of PD and how to detect them [15].

2.2.1 Dissolved Gas Analysis

Dissolved gas analysis (DGA) is mainly used by the industry nowadays to continuously monitor the traces of gasses within different HV equipment. Monitoring the level of different gases produced at the breakdown of dielectric insulation is done in this process. There are several ways of using the DGA, the simplest of which is by taking samples of the oil insulation from HV transformers and analyzing them in the lab. Some of the monitored dissolved gases are acetylene (C_2H_2),carbon dioxide (CO_2), hydrogen (H_2), methane (CH_4) and ethylene (C_2H_4). Each gas is emitted from a different type of PD activity within the oil-filled transformer.
Some other devices have a built-in gas sensors that can provide readings regularly. This method is used in conjunction with Condition Based Maintenance to monitor old HV power transformers.
These type of dissolved gas analysis has its advantages and disadvantages:

Advantages:
- Estimate the life expectancy and health of power transformer in insulated oil
- Identify the PD type

2.2.2 Acoustic method

PD activities generates tiny bursts in the surrounding medium, which in turn generate mechanical waves that propagate through the medium until they reach a barrier. These waves contain a wide range of acoustic frequencies. The higher frequencies are attenuated faster than the lower frequencies the further they travel due to energy loss in the surrounding material. The most common sensors used in acoustic measurements are the piezoelectric sensors. They operate by converting mechanical vibrations into electrical signals and they are also used in the opposite manner as computer clocks and oscillators. The detected PD signals can be affected by several factors as they propagates from the source to the sensor. Some of these parameters affecting acoustic waves are: attenuation factors through different propagation media, reflections, type of sensor and PD type and distance from sensor[18].

Advantages:
- Does not require a complete shutdown of the HV device (On-line method)
- Unaffected by ambient electromagnetic interferences
- Can be mounted on solid boundaries of HV systems without any special installation requirements
- Can be used for localization of PD sources

Disadvantages:
- Low sensitivity to PD sources within oil tanks depending on the type of sensor used and location of the sensor with respect to the PD source
- Prone to signal attenuation, reflections, mechanical noise and reverberations
- The presence of solid barriers within the oil-filled transformer (core, windings, and structural supports) causes additional propagation difficulties

2.2.3 Optic Method

The optic method utilizes light emissions radiated from the PD source to the optic sensor. Intense partial discharge activities produce flashes of light as the dielectric around them is ionized and electrons flow due to an intensified electric field. In the paper written by B. Song et al. the authors implemented an array of silicon photomultipliers that would be inserted into a gas insulated switcher (GIS) [20]. The sensor is used to detect photons released from a PD source inside the GIS system.

In another paper by B. Dong et al. a different sensor was used to capture optical emissions of a PD. The cavity within the sensor was filled with SF_6 in order to increase its resistance to high voltage stress during in-situ testing within transformers [5].

A different kind of sensor that utilizes fiber optic cables but not optical emissions is a fiber coated with a bragg grating (FBG). The FBG sensor instead converts mechanical vibrations and pressure into opto-acoustic signals that can be transmitted across the fiber and then digitized. Since the PD emission is essentially a miniaturized break down of insulation, it generates pressure waves that travel in the medium until they reach the boundaries of the HV device, typically a metallic wall. If the FBG sensor was placed on the metallic wall, it would be able to detect the incoming waves through vibrations within the wall and in turn translate them into PD signals [12]. The FBG operates similarly to a typical acoustic sensor but has a much higher sensitivity to vibrations.

Advantages:
- Has a stable output
- Fast response time
- High SNR
- Can be used for PD localization

Disadvantages:
- Optic devices are usually expensive and sensitive
- High sensitivity to temperature
- Requires a stable distributed bragg reflector laser (DBR) as a source
- The opaqueness of the dielectric liquid insulation such as insulation oil limits the propagation of optic waves in its environment due to its high refractive index
- Must be installed during the production stage of the transformer

2.2.4 Electrical Detection Methods

Besides the aforementioned effects of a partial discharge within a HV device, a PD shows electrical and electromagnetic signs as well. For example, PD occurrence generate a high frequency current that goes towards ground; detecting this current can confirm whether a PD has occurred or not. To be able to detect such manifestations, a high frequency current transformer (HFCT) is connected to the ground lead of a HV transformer. HFCT can be effective in detecting PD signals but the downside of using them is that they have a relatively slow response time for a fast rising PD pulses, i.e.: PD signals with pulses of several hundred nano seconds in length [4].

Advantages:
- Online detection method
- Not affected by other sources of interference if ground is properly isolated
- The detected PD signal is less distorted in other wireless detection methods

Disadvantages:
- Slow response time for fast rising PD pulses
- Has a limited detection frequency band

2.2.5 Classical PD Measuring System

Classical PD measuring systems have been standardized and used by the industry for more than 50 years. The detection system shown bellow in figure 2.5 was taken from (CIGRE-2008-2), where each part of the system is labeled. Starting with the input at the left side, where the PD pulse feeds into the system, the signal goes through an attenuator or a voltage divider (1) so it can be handled by the internal circuitry. Then, an amplifier (2) boosts the detected PD signal, which is then passed on to band-pass filter (3) that would omit frequencies outside the range of interest. The IEC 60270 uses two types of band-pass filters, narrow-band with $\Delta f = 9 - 30\,KHz$, or a wide-band with $\Delta f = 900\,KHZ - 30\,MHz$. After passing the PD pulse through the filter it goes towards a peak detector circuit (4) where the PD intensity level is detected and transferred to the indicating instrument (5). The PD pulse can also be examined based on its location in degrees with respect to the synced AC voltage signal, which can be viewed in the visualization unit (6) [7].

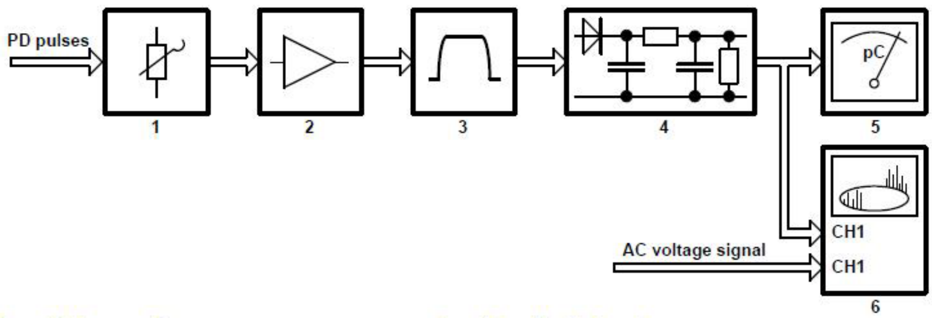

Figure 2.5: classical PD detection system [7]

2.2.6 Ultra High Frequency Emissions

Other literature sources recommend the utilization of ultra-wide band antennas to detect the electromagnetic emissions of the PD pulses. It is convenient because it is one of the online detection methods. This is still a relatively young process when compared to other PD detection methods; thus, there are many interesting antenna designs in the literature that show great promise in this field [1]. Since PD pulses are very short impulse signal in time, it is presumed that they have an ultra-wide frequency band containing all of the pulse‘s energy. Therefore, if one wants to capture most of the PD signal, one must obtain all the frequencies contained within the PD impulse signal. According to Coenen and Tenbohlen, the range of frequencies emitted by a PD pulse in the ultra-high frequency (UHF) range is estimated to be within 300 MHz-6 GHz [2]. Research also showed that among all other detection methods, UHF detection methods show relatively good results when it comes to sensitivity. Also, when it comes to signal to noise ratio captured by the antenna, UHF has the best results in oil-filled transformer tanks. This is due to the fact that the tank is shielded from all sides with metallic walls that work as a Faraday‘s cage [2][3][19]. The main disadvantage of using the UHF method is finding a proper insertion method or a place that does not contain a conducting material as it will block the antenna from receiving any PD emission from within the transformer tank. Thus allowing the EM signals to propagate from the PD source and towards the antenna outside the tank. New power transformers are built with dielectric windows distributed along the walls, but when it comes to old units, other methods must be considered [7]. This can limit the ability to localize PD sources as it requires placing several sensors around the tank.

Advantages:

- Relatively small and compact size
- Easy and cheap to manufacture the sensor
- Fast response time
- High SNR in oil-insulated power transformers
- Can be used for PD localization
- Can be designed to have an ultra-wide detection band
- Patch antennas usually have a hemispherical radiation pattern allowing them to detect PD sources from all angles with equal gain

Disadvantages:

- Requires an insertion or mounting method
- Design of ultra-wide band antennas is complex
- May require an expensive data acquisition unit for high frequency digitization

2.3 Antennas Used for UHF PD measurements

Finding the optimal antenna design for PD detection was and still is the center of attention for many researchers in this field. Designing, manufacturing and testing several types to investigate their performance in lab or actual testing environments lead to many discoveries in this field. Currently, industries use monopoles with length of 5-10 cm for old transformers, these monopoles resonate at frequencies above $1GHz$ [17]. Another antenna design, the log-periodic antenna, can be used for detecting frequencies below $750MHz$ but not above that range [17]. Patch antennas are very simple devices and may be the best suitable option for such an application. Made of a specific pattern on a printed circuit board (PCB) and mounted with a feeding component. One of the most promising patch antenna designs is the Hilbert fractal antenna. The HFA is interesting for PD measurements since it has an ultra-wide band of resonant frequencies capable of capturing many frequency components along with its compact size and its high sensitivity to PD pulses [10][25].

Industrial solutions have been suggested for inserting antennas inside operational oil-filled transformers. Figure 2.6 shows one of the intrusive methods used for inserting a UHF antenna through the drain valve suggested by **OMICRON**, usually located at the bottom of a transformer [7]. The location of the drain valve is suitable for PD measurements and allows scanning in the whole transformer, since the HFA sensor has a wide radiation pattern that will be further discussed in the following sections. By insuring that the designed antenna is within a certain diameter, smaller than the drain valve, this insertion method can be applied.

Figure 2.6: UHF antenna inserted in the oil drain valve of a HV transformer [7]

2.3.1 Hilbert Fractal Antenna

Fractal antennas employ fractal geometry in their design to produce a micro-strip antenna. These fractal geometries are self-symmetric by nature which leads to a realization of multi-frequencies resonance of the design [23]. Another reason for using a fractal curve is its natural ability of plane-filling that allows it to increase in length as the order increases while having the same constant area. Different types of fractal antennas meet the aforementioned criteria, the Koch, Penao and Hilbert curves share the same features, which in turn provides an improved frequency response [10]. In figure 2.7 the effect of increasing the order of the curve is shown to increase the overall length of the curve as well. Therefore, as the order increases the number of resonant frequencies increases and the lowest resonant frequency decreases [13].

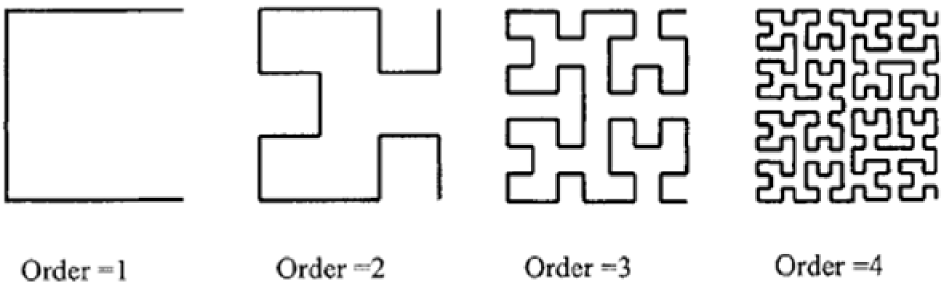

Figure 2.7: Hilbert curves with different orders.

2.3.2 Operational Bandwidth

The designed antenna is expected to capture more energy from the partial discharge since it is modeled to have an ultra-wide band response. As figure 2.8 shows, the left graph shows the delta function in time, while the graph on the right shows its Fourier transform in frequency domain. A perfect delta/pulse function in time has a flat frequency spectrum across all frequencies. Each frequency component contains a part of the signal‘s energy; thus, collecting as many frequency components as possible may provide more information and insight into the PD phenomena. It also means that the sensor may have higher sensitivity to PD activity since it can detect more energy from each PD emission.

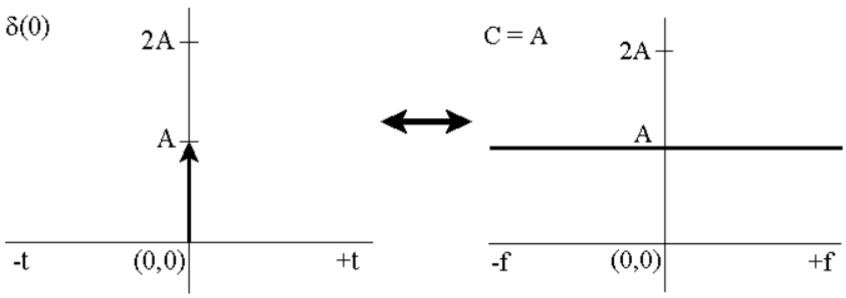

Figure 2.8: Fourier transform of a Delta in time [14].

Several sources mentioned that the partial discharge contains frequencies between 300 MHz-3 GHz[2]. The lower limit is set to distinguish actual PD activity from any corona that may be generated in the bushing or other external sources, while the large bandwidth shows higher sensitivity to PD emissions [10]. With that in mind, the antenna design will be optimized for the purpose of having an ultra-wide band, while maintaining a compact size.

In order to estimate the resonant frequencies of the antenna, the **S11** parameter will be investigated in the design stage. The S11 parameter refers to how much power would be reflected from the antenna feeding point back at the antenna itself, hence, its name **reflection coefficient** or **return loss**. The S11 parameter is frequency-dependant, which means that it might have different values for each frequency. That does not mean that he reflection coefficient is a function of the frequency, but rather more dependant on the design of the antenna itself. For example, if the reflection coefficient $S11(f) = 0\,dB$ then all the power from the signal is reflected and nothing is radiated or passed to feeder, i.e.: no resonance at this frequency. On the other hand, if $S11(f) = -10\,dB$ and if the incoming power equals $5\,dB$ then only $-5\,dB$ will be reflected and the rest will be transmitted. This is shown by figure 2.9 at $f \approx 0.8\,GHz$ the $S11 \approx -35\,dB$, which means the antenna is good at received that specific frequency; whereas, as the frequency deviates from $f \approx 0.8\,GHz$ the value of S11 increases until it reaches $-10\,dB$ which signifies the threshold for acceptable S11 values. These two points tagged at the $-10\,dB$ threshold line indicate the operational bandwidth of the antenna in question.

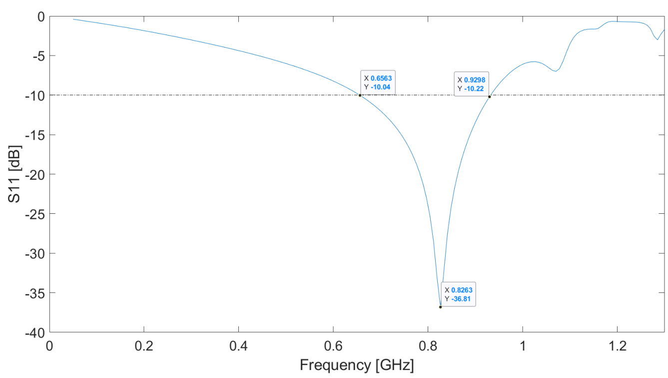

Figure 2.9: S11 parameter vs frequency.

2.3.3 Radiation Pattern of the Hilbert Antenna

In addition to the operational bandwidth, another very important criterion of an antenna is its **radiation pattern**. Basically, it is the graphical representation of the radiation intensity as a function of the azimuth and elevation angles in space, representing the power radiating from the antenna. It is usually observed at the far field of an antenna, where the far field is a measure of the distance far from the antenna where the radiation does not change shape with distance. There are three main types of radiation patterns:

- Isotropic: radiates equally in all directions
- Directional: radiates or receives signals more effectively in one direction than in others
- Omni-directional: radiates isotropically in one plane and directionally in any orthogonal plane

An isotropic radiation pattern is not physically attainable as it originates from a point source and radiates equally in all directions, thus it is used as a standard measure of radiation gain with units of dBi, db with respect to isotropic radiation.

A typical directive radiation pattern is shown in figure 2.10 below where the main lobe, side lobes and the back lobes are shown in the 2-D graph. The main lobe is usually the most important part in the radiation pattern of an antenna, side and back lobes are extremely undesirable and the design is usually optimized to reduce their effects or remove them completely.

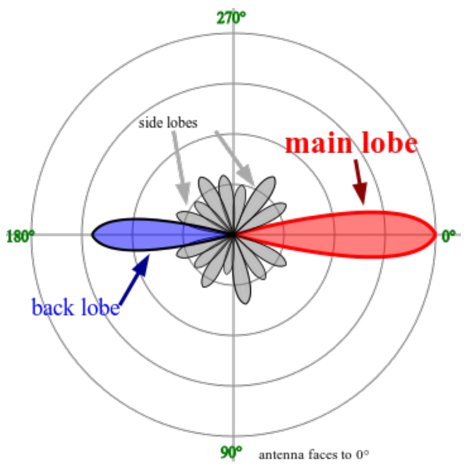

Figure 2.10: Radiation Pattern.

For the purpose of PD measurement and analysis, a directive radiation pattern is preferable as it allows for equal scanning in all directions with equal gain and no dependency on the angle. Figure 2.11 shows what the antenna radiation pattern is expected to look like. This is what a patch antenna is expected to have, a hemispherical main lobes with nearly equal gain from all sides as well as back or side lobes significantly smaller than the main lobe.

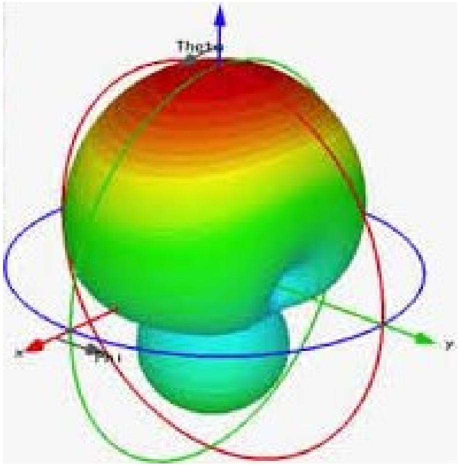

Figure 2.11: Hemispherical radiation pattern.

2.3.4 Design Assumptions and Criteria

As mentioned previously, the antenna will be designed to have an ultra-wide band in order to capture most of the PD pulse and to fit in a $10\,cm$x$10\,cm$ square area in order to achieve compactness in size, which would later be beneficial while installing the antenna inside or outside a HV transformer. The performance of the Hilbert antenna is affected by the following factors:

- The side dimension of the PCB (L)
- The order of the antenna (n)
- Width of the patch antenna conductor (b)
- Thickness of the PCB substrate (t)
- Location of the feed point of the antenna
- Type of feed used
- The relative permittivity of the PCB, expressed with ϵ_r

To formulate the design of the Hilbert fractal antenna, the resonance of the meander line, shown in figure 2.12, will be used as reference. For each segment of the meander line, the equivalent inductance will be calculated, while considering each segment as a "short circuit parallel two-wire line". Then, the total inductance will be compared to that of a regular half-wave dipole. This approximation was reported by [6] and [22], where their formulation can be extended to include the design of a Hilbert fractal antenna.

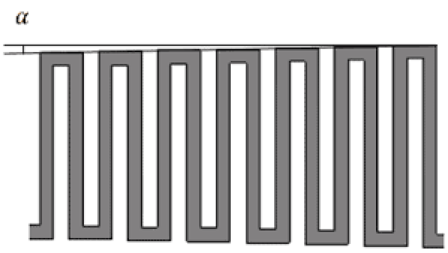

Figure 2.12: Illustration of the meander line antenna.

The following equations will be used to retrieve the initial parameters of the Hilbert fractal antenna that would satisfy the aforementioned criteria. For an antenna with an outer dimension of $l = 10\,cm$ and an order $n = 4$, the length of each line segment (d) can be calculated using equation (2.1)

$$d = \frac{l}{2^n - 1} = 6.667\ [mm] \approx 6.7\ [mm] \tag{2.1}$$

Thus, the overall length of the segments not forming the parallel wire of the HFA curve will be described by S in equation (2.2)

$$S = (2^{2n} - 1)d = 846.7\ [mm] \tag{2.2}$$

The characteristic impedance of a wire segment with length d and width b is denoted by equation (2.3). Thus making b equivalent to $1.223\,mm$ in order to have a matching impedance $Z_0 = 50\,\Omega$.

$$Z_o = \frac{\eta}{\pi} \log(\frac{2d}{b}) \tag{2.3}$$

where η is the intrinsic impedance of free space denoted by $\eta = \sqrt{\frac{\mu_o}{\epsilon_o}} = 377\ \Omega$, $\eta_{copper} = \frac{\eta}{\sqrt{\epsilon_r}}$ and ϵ_r for copper is around 6.2

The aforementioned calculated antenna parameters will be used to design the HFA and analyze its response to check its applicability for PD acquisition.

3

Methodology

3.1 Typical PD Detection System

To detect PD activity in any HV system, a typical detection and measurement system that follows the *IEC* 60270 standard can be used. The system architecture and components are shown in figure 3.1, which will be discussed in details below. The detection system is divided into three parts, **PD generation**, **typical PD detection system** and **UHF detection system**. Components (1-6) within the typical PD detection system are explained in section 2.2.5.

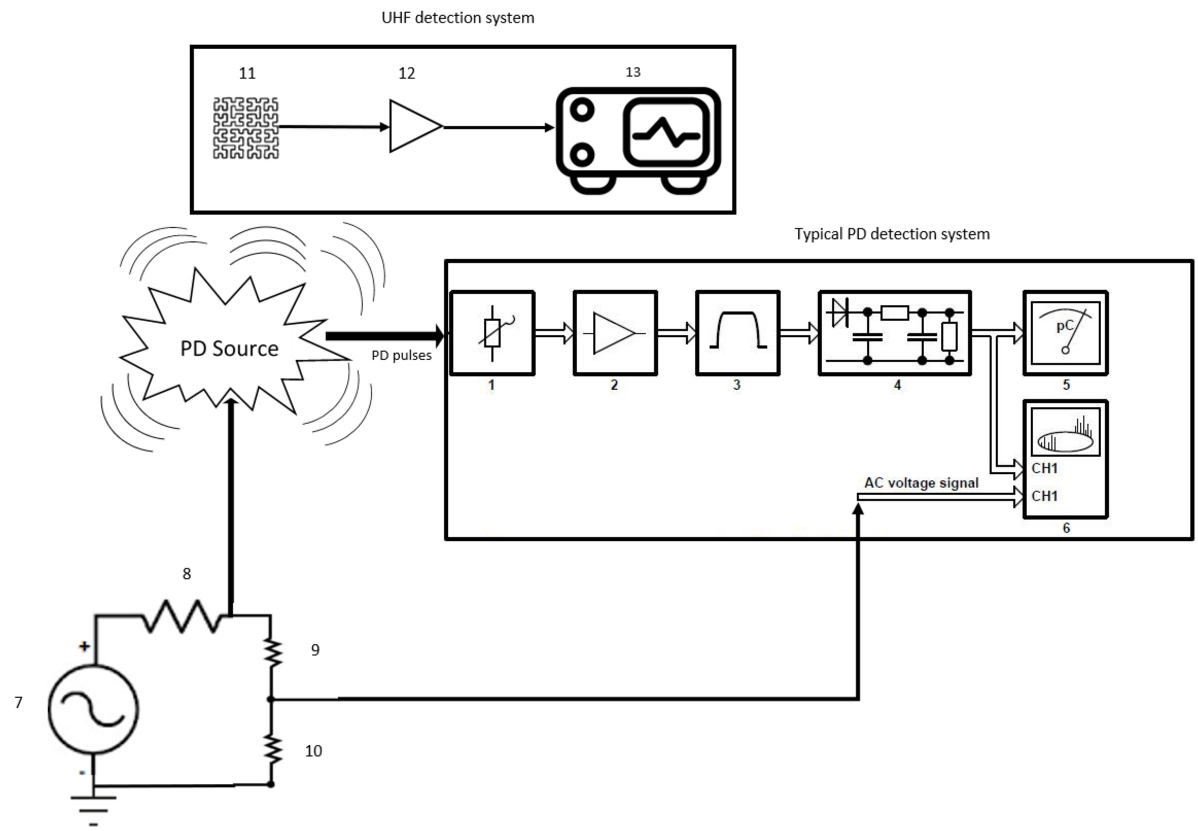

Figure 3.1: PD testing and measuring setup.

The system is energized by controlling the AC source (7) which connects to a current-limiting resistor (8), that would restrict the maximum PD intensity level at the PD source. Components (9 and 10) depict the resistances for the voltage divider, used to reduces the amplitude of the AC signal going to the PD detector, which will be used as a synchronizing input for the PD measurement. After energizing the PD source, electromagnetic emissions are radiated in all directions, by placing the Hilbert antenna (11) in proximity to the PD source, those emissions can be detected by the HFA. The signal collected by the antenna is very weak at this stage to the point that it can barely be distinguished from the ambient noise. To improve the signal of interest to noise ratio, a low noise amplifier (12) is placed after the antenna, which would boost the signal by 32 dB. Finally the boosted signal would travel to the oscilloscope (13) to be digitized and stored for further processing. The UHF and typical PD detection systems are used simultaneously to collect information about the generated PD signal. Using both systems in this configuration would assist in estimating the sensitivity of the Hilbert fractal antenna towards PD activity.

3.2 Testing Stages

To perform PD analysis and testing, the process will run through several stages. The stages are meant to build a baseline for the sensor and confirm the operational parameters of the antenna to make sure everything is working according to the designed values. The procedure will be divided into three stages, each stage will add more life-like components to simulate the real life HV transformer in which PD will be monitored. The stages of testing are PD sources in air with the antenna placed in proximity and PD sources submerged in an oil-filled tank with the antenna placed inside the oil.

3.2.1 Stage 1: Verification of Process

In this stage, the antenna was set in air to detect various PD sources with known PD intensity that will be measured using the typical PD detection circuit. The purpose of this procedure was to find a relationship between the captured signal energy and the PD intensity that was detected by the measuring device. Thus, giving the antenna a plane of reference that would help in estimating the sensitivity and effectiveness of the antenna.

Three different PD sources were used in this stage, twisted pair, sharp and void. Figure 3.2 shows the twisted pair wire strip used to generate PD. The wires are made of a copper conductor covered with Polyamide-imide as an insulation layer. The diameter of the each wire was around 1 mm and the number of twists made were 13 twists, with a spacing between each twist equal to almost 1 cm. The edges on the left are curled back at the ends of the wire to reduce the effects of corona as the ends are sharp points while the branching ends on the right side are stripped of their insulation so they may be connected to the HV leads when energized.

Figure 3.3 shows the device used to generate a sharp PD signal; the components of the sharp PD source were simply a sharp edge represented by the needle on the left, which is connected to ground, along with a metal sheet connected to HV. Arching

Figure 3.2: Twisted pair PD source.

between the two conductors is classified as a sharp point discharge. The source generates PD when the electric field intensity on the tip of the needle exceeds the limits of the insulation medium, generating a partial discharge of flowing electrons from high potential to ground. Sometimes, the PD intensity is too high for this PD type, to reduce the intensity to a readable and stable level, a limiting resistor between 100 $M\Omega$ to 300 $M\Omega$ was added to the PD source.

Figure 3.3: Sharp PD source.

The void PD, shown in figure 3.4, is made by placing two separated conductors within an enclosed environment with some space between them. In this case the two conductors are enclosed within a plastic rod and a hole was drilled to allow the two conductors to be placed. The separation between the conductors creates an air bubble that isolates the two metallic connectors. A sealant is added at the outside of the rod where the conductors are placed to insure their mechanical stability and isolate the interior from outside interference.

Tests done using these PD sources in this setup were called **in air** and all the corresponding results were related to that notation. Figure 3.5 shows the test setup in air, with the HFA suspended around 30 cm from the PD source.

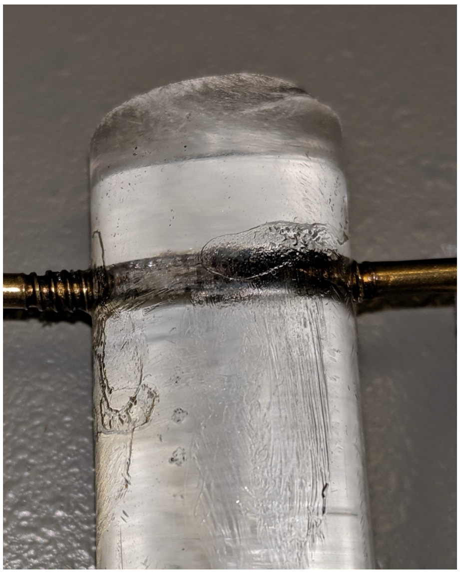

Figure 3.4: Void PD source.

Figure 3.5: Sharp PD test done in air.

3.2.2 Stage 2: Oil-filled Test Tank

The second stage of the testing process requires utilization of an oil-filled tank that was used to submerge both the antenna and the PD source. All tests done inside the oil tank were noted as **in oil**, and this notation was used throughout the process. Figure 3.6 shows a sample of the test done inside the tank, where both the antenna and the void PD source are placed under the oil surface. Thus, changing the effective primitively of the medium $\epsilon_{r,Oil}$ and modifying the response of the antenna. The purpose of this test was to simulate what would happen to the antenna and detected PD signals if the antenna was placed inside a real oil-filled HV transformer. As mentioned before, the antenna is expected to have a better response under oil, which in turn indicates that the results acquired from this test should show better performance in terms of sensitivity to PD activity.

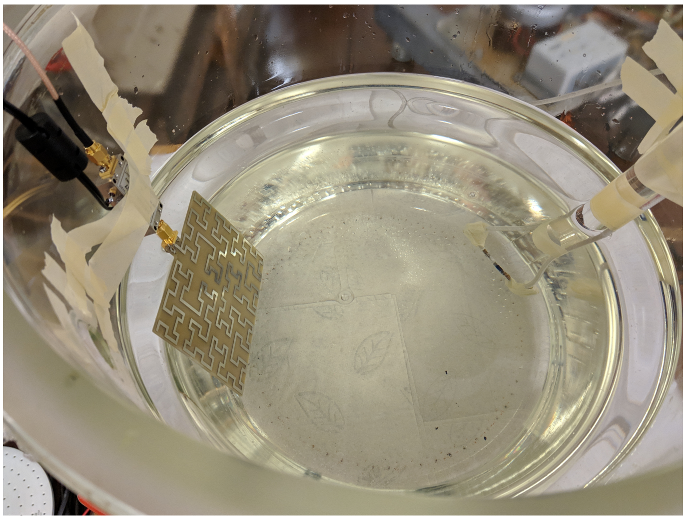

Figure 3.6: Void PD tests inside an oil-filled tank.

3.2.3 Sensitivity Tests of PD Sensors

The purpose of this study is to investigate the Hilbert antenna as a PD sensor with reference to the IEC 60270 standard. The way to do so with the aforementioned setup is to find the correlation between the PD intensity level taken from the **PD Detector** and the energy of the signal capture by the antenna. Finding this correlation factor at different stages of the process would allow a comprehensive analyses of the sensor and establish a base for UHF sensor calibration for PD detection.

3.3 Equipment

3.3.1 Low Noise Amplifier

The LNA is one of the most important component in the radio frequency (RF) stage. Having an LNA means that the captured signal is amplified while keeping the noise level at a minimum. The trade-off with typical RF amplifiers is that they add their own noise due to their internal temperature. Low noise amplifiers are designed to have less noise added to the signal; thus increasing the SNR level. The LNA used was chosen based on its frequency range which is $9KHz$-$3GHz$. The gain of the LNA throughout the frequency range is shown in figure 3.8 where it can be seen that it is sufficiently flat. This performance and flatness is very good for such an application because it provides similar amplification rates for all frequency components. The gain of the amplifier is 32 dB and the flatness across the range is ± 1.25 dB. The low noise figure value indicates that not much noise has been added to the signal as the SNR difference between the input and the output represented by the noise figure is just $F = 2.5\,dB$, refer equation (3.1). Thus, the effective temperature of the device at room temperature $T_o = 300\,K$ is $T_e = 233.5\,K$, taken from equation (3.2). Showing that the effective temperature is a relatively low value for an amplifier with such a wide range and high gain compared to several $1000\,K$ for a typical amplifier of the same range. Note that the effective temperature of an amplifier indicates how much noise it adds to the signal, where higher effective temperature means more noise added. Finally, since standing waves occurring within the amplifier may overheat it, since amplifiers response are usually temperature dependant, it might alter its performance. Thus, the reverse isolation between signals traveling from the output towards the input is $55\,dB$, which is significant enough to reduce the effects of standing waves within the device.

$$F = \frac{SNR_i}{SNR_o} \tag{3.1}$$

$$T_e = (10^{F/10} - 1)T_o \tag{3.2}$$

Figure 3.7: Low noise amplifier.

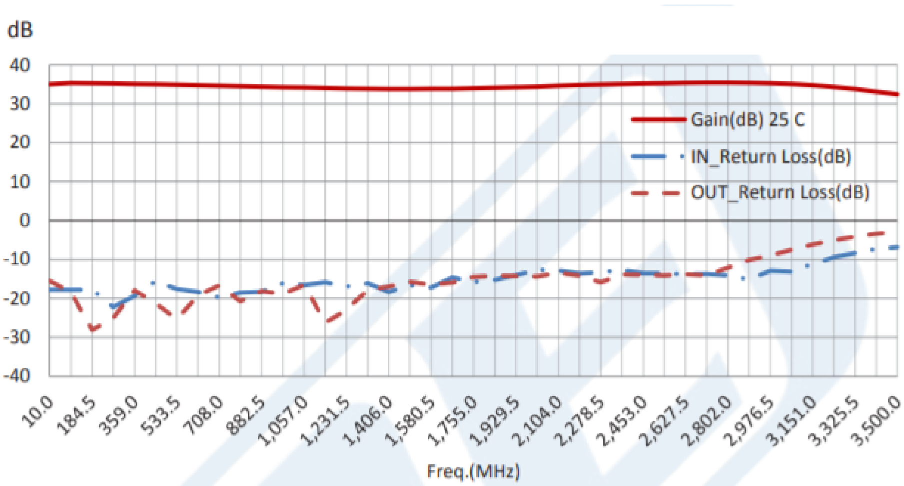

Figure 3.8: Gain of the LNA in Vs Frequency [21].

3.3.2 Oscilloscope

Choosing a suitable oscilloscope for a measurement setup is crucial in order to acquire signals containing the required range of frequencies. The oscilloscope used in this study was **LeCroy WaveRunner 620Zi**, capable of digitizing signals with an analog bandwidth of up to 2 GHz. Having such capabilities along with the wide band LNA and the Hilbert antenna allows for the maximization of captured energy from the PD phenomena. The oscilloscope‘s functions also enables the instantaneous processing of digitized signals, giving the option of online processing of captured PD signals.

Figure 3.9: LeCroy WaveRunner 620Zi oscilloscope.

4

Results

4.1 HFSS Simulation

To be able to understand how the HFA is working and to examine its response and capabilities, a model was designed using ANSYSS - high frequency simulation software (HFSS). Using this software, the antenna was tested for different parameters, namely gain, S11, and directivity.

The optimum design was chosen based on the best resonant frequencies and the feeding point, where it had the following parameters:

- Order of the Hilbert fractal antenna ($n = 4$)
- The side dimension of the PCB ($L = 100\, mm$)
- The width of conductor segment of the patch ($b = 1.223\, mm$)
- The thickness of the PCB ($t = 1.5\, mm$)
- The dielectric constant of the FR-4 PCB ($\epsilon_r = 4.4$)
- Coaxial feeding method ($Z0 = 50\Omega$)
- SMA mount as feeding type

4.1.1 S11 Parameter and Operational Bandwidth

4.1.1.1 Analysis in Air

Figure 4.1 below shows the simulated 4th order Hilbert antenna, where the drawn pattern is the conductive patch and the background green surface is the FR-4 PCB layer. The feeding point is indicated by the red circle showing the location of the feed of type SMA.

The return loss of the antenna was examined at two stages. The first using HFSS to simulate the resonant frequencies and the second using a vector network analyzer (VNA), which tests the manufactured antenna and returns the S11 parameter. A comparison between the two would show the difference between theoretical and tested parameters and shed light on what caused the differences. As mentioned before in section 2.3.2, the threshold limit for acceptable $S11$ values is at $-10\, dB$ or less, giving low reflected signal levels and appropriate transmitted signal. All figures bellow include a dashed line "$--$" showing the threshold for the operational

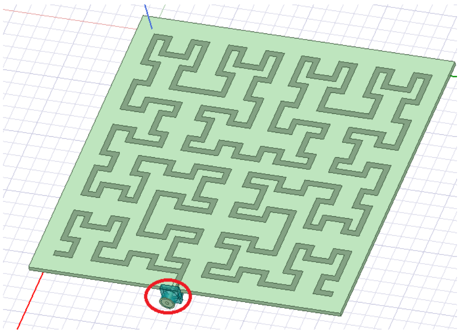

Figure 4.1: The simulated 4th order Hilbert antenna.

bandwidth of the antenna, where values below that threshold will be included in the bandwidth of the sensor. Figure 4.2 illustrates the S11 response of the antenna taken from HFSS. The figure spans from 10 MHz to 3 GHz, where the operational bandwidth of the Hilbert antenna shows a multi-band response spanning the whole range.

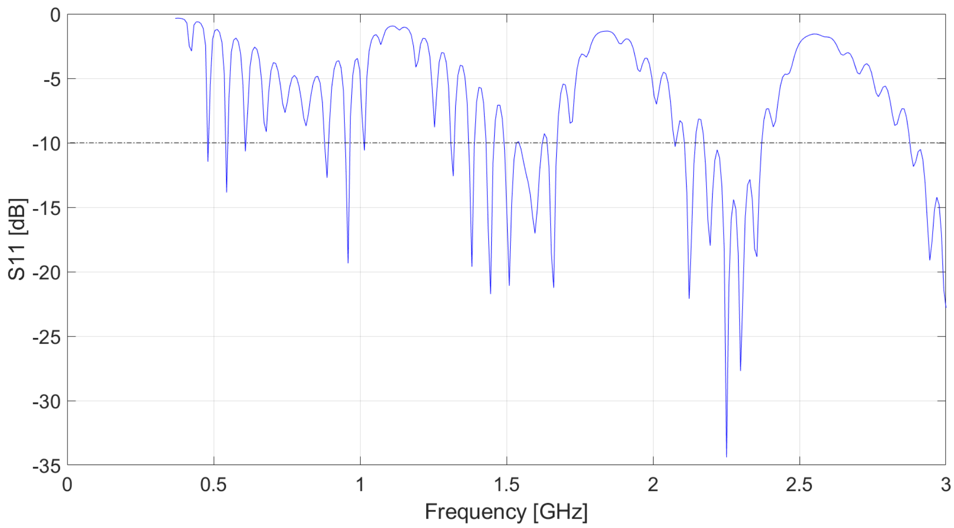

Figure 4.2: Simulated S11 parameters Vs frequency for the Hilbert antenna, where the dashed line shows the threshold set to -10 dB.

Almost the same response is depicted in figure 4.3 where the manufactured HFA shows similar performance to the simulated graph, with respect to the S11 parameter, tested in air, as shown in figure 4.4. The antenna is placed in free air to test its frequency response using the VNA.

To be able to understand the similarities and differences between the simulated and tested S11 graphs, figure 4.5 shows an overlaid version of the two graphs where the resonant frequencies are almost identical in location with slight variation in magnitude and non-linear frequency shift that starts from 1.5 GHz onward.

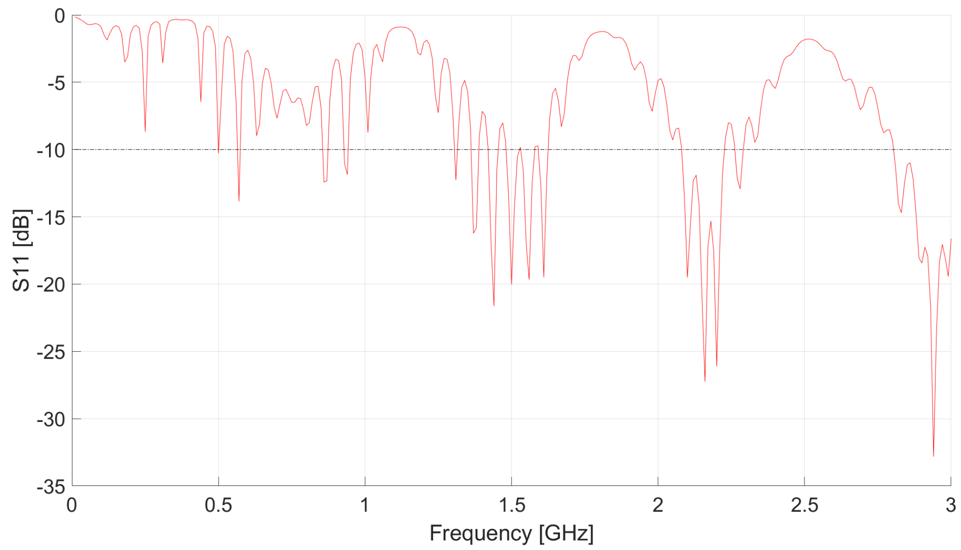

Figure 4.3: Tested S11 parameters Vs frequency for the Hilbert antenna, with -10 dB threshold.

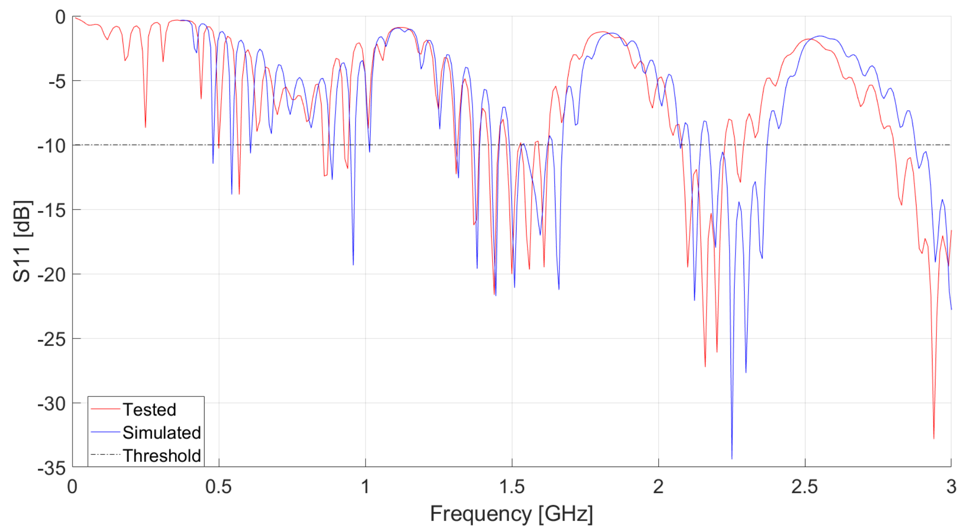

Figure 4.5: Overlaid S11 for test and simulation of the Hilbert antenna for comparison, with -10 dB threshold.

The resonant frequency matching between the simulated and tested S11 shows that the design of the Hilbert antenna was successful and follows the theoretical equations used to obtain it. The variability in magnitudes between different similar resonant frequencies between the two figures might be caused by environmental changes and ambient noise sources in the testing environment, that were non-existent in the simulation setting. Moreover, the non-linear frequency shift between the two graphs shows that the manufacturing process was not perfect, as the tolerance or deviation in designing the PCB might be insignificant to certain applications, it is not the same for UHF frequencies. This is due to the facts that the wavelength is so small

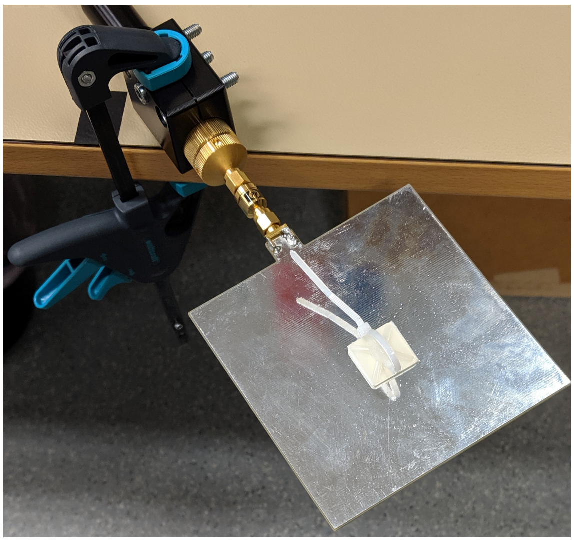

Figure 4.4: Hilbert antenna test setup in air, pointing downwards to mitigate the effects of EM waves in the lab.

at 1.5 GHz-3 GHz that the surface roughness and finishing must be $\leq \frac{\lambda}{10}$ or smaller to have the appropriate response from the antenna. This cannot be mitigated, but is still acceptable, since the antenna contains separate bands. A slight shift in these bands will not affect the PD acquisition process, as capturing as many frequency components as possible from the PD source within the 300 MHz-3 GHz range is the goal of this antenna design.

To summarize the results, the operational bandwidth will be contained in several bands, across the region of interest, i.e.: 300 MHz-3 GHz, which is detailed in table 4.1 and taken from figure 4.3 at $-10\,dB$ threshold. It can be clearly seen from the table that the bands are slightly small compared to the overall range in question; however, one must remember that the threshold is set at $-10\,dB$ which is usually considered a harsh benchmark for an antenna. This is why table 4.2 shows the estimated bandwidth of the antenna if the threshold was reduced to $-6\,dB$ instead, and the corresponding graph will be portrayed in figure 4.6. Table 4.2 shows that bands $1, 2$ have been merged after the threshold was relaxed to $-6\,dB$, given only 4 bigger bands, instead of the 5 smaller bands at threshold $-10\,dB$.

Table 4.1: Multi-band response of the Hilbert Antenna at -10 dB threshold

Band No.	Start [GHz]	End [GHz]	Bandwidth [MHz]
1	0.56	0.58	20
2	0.85	0.95	100
3	1.3	1.63	330
4	2.08	2.29	210
5	2.8	3	200

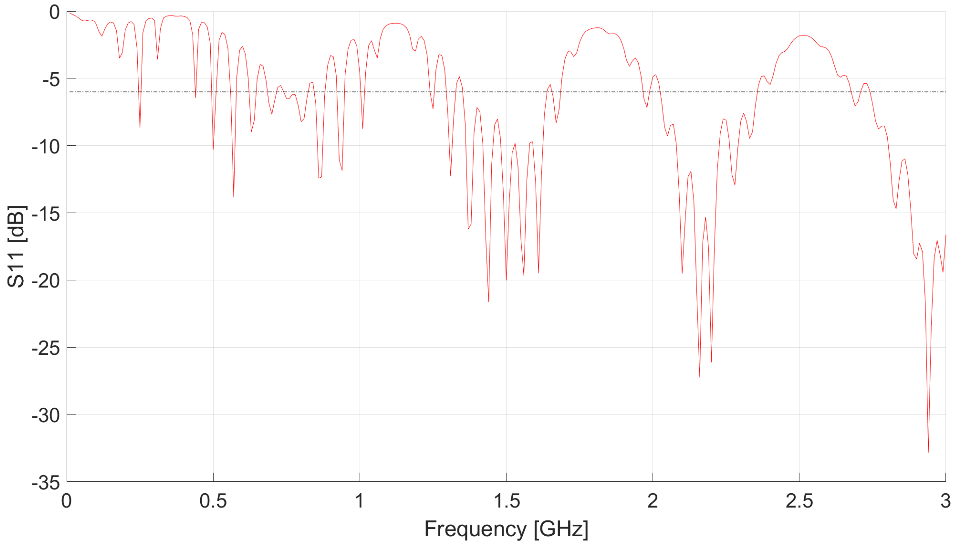

Figure 4.6: Tested S11 parameters Vs frequency for the Hilbert antenna, with -6 dB threshold.

Table 4.2: Multi-band response of the Hilbert Antenna at -6 dB Threshold

Band No.	Start [GHz]	End [GHz]	Bandwidth [MHz]
1	0.24	1.02	780
2	1.24	1.69	450
3	1.96	2.36	400
4	2.67	3	330

One can use the operational bandwidth for each threshold level as a ratio with respect to the overall frequency range. The ratio can be computed using formula (4.1), giving a value of $\eta_{-10} = 28.7\%$ for $-10\,dB$ and more than double that with $\eta_{-6} = 64.3\%$ for $-6\,dB$. The coverage of the first case is considered acceptable for such a wide range of frequencies, while the coverage in the second case with a threshold of $-6\,dB$ showed more coverage percentage around the frequency range of interest. This shows great promise and proves that the Hilbert antenna is suitable for this application.

$$\eta = \frac{\sum Bandwidth_{Band(i)}\,[GHz]}{3\,[GHz]} \tag{4.1}$$

where i is an integer index that is $i = 1, 2, 3, 4, 5$

Thus, it can be seen that the operational frequency of the designed antenna can be subjective and dependant on the threshold set for S11. The actual captured frequency components will be shown clearly from actual samples of captured PD signals.

4.1.1.2 Analysis with an Oil-filled Tank

To further investigate the HFA frequency response, the following tools, figure 4.7, were used to mimic different environment or settings where the antenna could be used. The tools would simulate the oil environment inside a real HV transformer, a dielectric windows on a transformer tank and a metal enclosed tank that would add many reflections and multipath effect to the antenna response and change its radiation pattern.

Figure 4.7: Antenna testing tools.

To further illustrate the testing setup, figures 4.8 and 4.9 show the testing tools, where the white bucket represents a dielectric window on the side of an oil-filled transformer and inside the bucket there is actual transformer oil. The antenna is placed on the lid in figure 4.8 so that its response will be affected by the plastic layer as well as the oil inside. On the other hand, in figure 4.9 the HFA is placed inside the oil bucket to simulate a complete submerging of the PD sensor in a transformer environment. One might argue that the bucket is too small and it does not contain objects that mimic the winding or the bushing that is present in a real transformer tank, but the response of the sensor here, the Hilbert antenna, is only affected by objects that are physically in close proximity to it, around 10-15 *cm*, otherwise, it will not have a major effect on the antenna.

Figure 4.8: Hilbert antenna placed on the oil container.

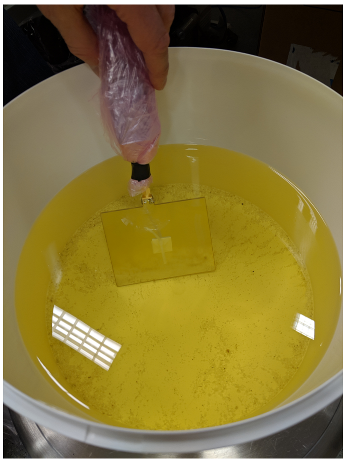

Figure 4.9: Hilbert antenna placed inside the oil container.

Therefore, the response of the antenna when placed on the oil container is depicted in figure 4.10. The S11 parameter shows no change between the antenna in air test and the antenna on the oil tank test. This indicates that the frequency response of the antenna stays the same when the antenna is placed on the dielectric window of a HV tank. Since the response of the antenna on top of the oil tank was similar to that of air, it can be assumed that the frequency bands and coverage matches with the results previously discussed in section 4.1.1.1.

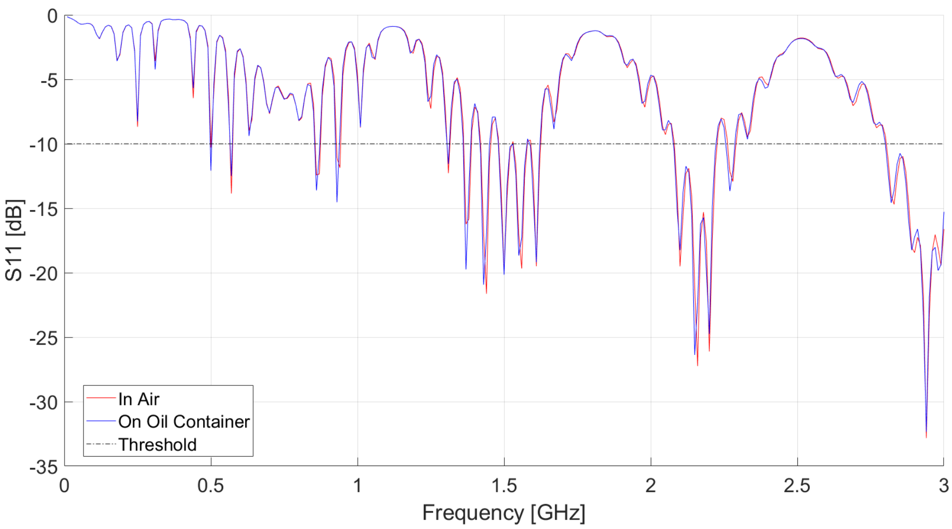

Figure 4.10: Overlaid S11 response of the Hilbert antenna in air (Red), on the oil tank (Blue).

A different response is created when the antenna is submerged in transformer oil. The S11 curve in figure 4.11 shows a non-linear down frequency shift of the curve belonging to the antenna when submerged with respect to its response in the air. Furthermore, the sensitivity of the antenna increases inside the oil environment, which is indicated by the increased peaks of the S11 graph (blue) showing less reflections at these frequencies, giving the antenna a higher sensitivity at these bands. Thus, the coverage bands shift and increase in percentage with respect to the overall range. The updated bands are shown in the following table 4.3 measured at $-10\ dB$ threshold. Using equation (4.1) giving a percentage coverage in oil, $\eta_{in\ oil} = 31.3\%$, which is clearly an improvement over the $\eta_{air} = 28.7\%$ taken from the antenna in air.

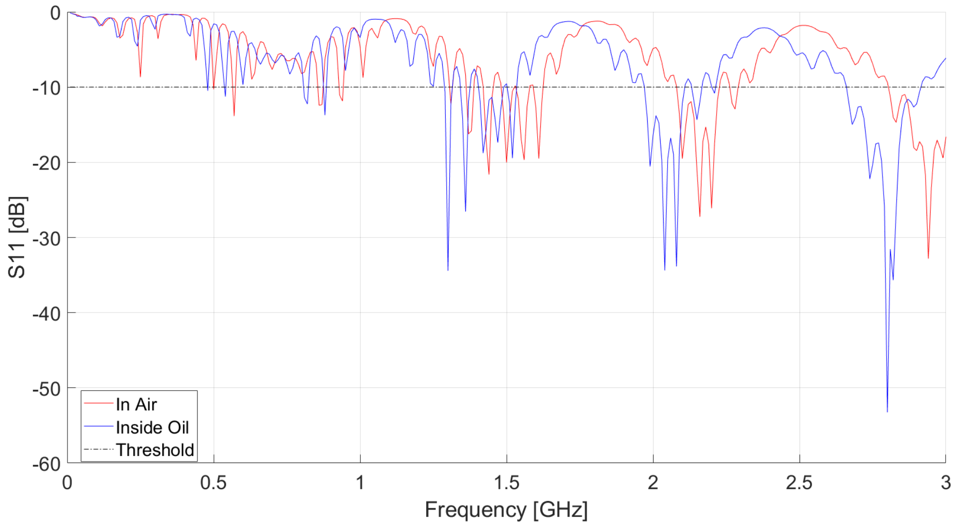

Figure 4.11: Overlaid S11 response of the Hilbert antenna in air (Red), inside the oil tank (Blue).

Table 4.3: Multi-band response of the Hilbert Antenna at -10 dB threshold inside an oil tank.

Band No.	Start [GHz]	End [GHz]	Bandwidth [MHz]
1	0.47	0.55	80
2	0.80	0.89	90
3	1.28	1.54	260
4	1.97	2.22	250
5	2.66	2.92	260

4.1.1.3 Analysis Inside a Metallic Tank

The previous part discussed mimicking an actual transformer tank, but what is a transformer tank without the metal shield covering it? The antenna was tested inside and outside a plastic container but not covered with a metallic wall. In this section, the same tests were performed with the addition of a metallic wall surrounding the test setup, shown in figures 4.12 and 4.13.

Figure 4.12: Hilbert antenna placed on the oil container surrounded by a metallic wall.

Figure 4.13: Hilbert antenna placed inside the oil container surrounded by a metallic wall.

The response from the antenna when placed on the oil container with a metallic wall surrounding it, figure 4.14, showed no deviation from that of the antenna in air, proving that the antenna is not affected by conducting surfaces that are not in close proximity as mentioned before.

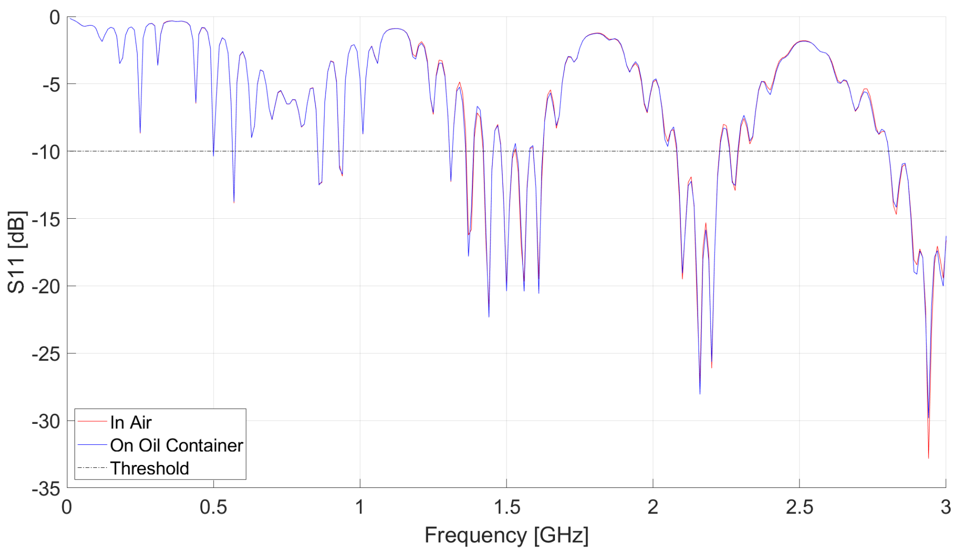

Figure 4.14: Overlaid S11 response of the Hilbert antenna of response in Air (Red) vs on the oil tank with metallic wall (Blue).

On the other hand, the response changed when the antenna was placed inside the oil container, figure 4.15, but still resembling the response acquired in figure 4.11 where the submerged antenna was not surrounded by metal.

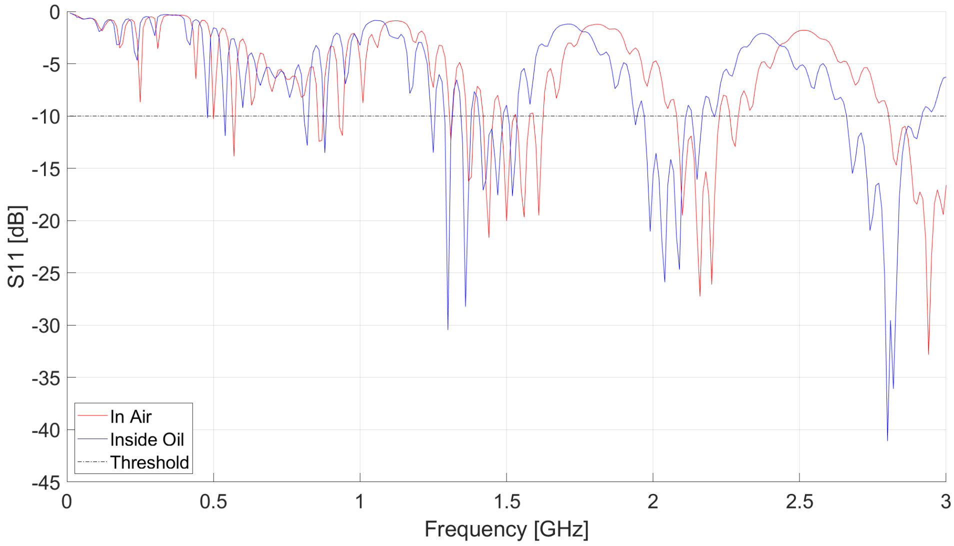

Figure 4.15: Overlaid S11 response of the Hilbert antenna in air (Red), inside the oil tank with metallic wall (Blue).

To confirm that the results for both with and without a metal wall are the same, figure 4.16 shows the responses of the antenna when submerged without a metal wall vs antenna submerged with metal wall. This indicates that both cases exhibited almost the same response as there was no significant discrepancy between the two curves.

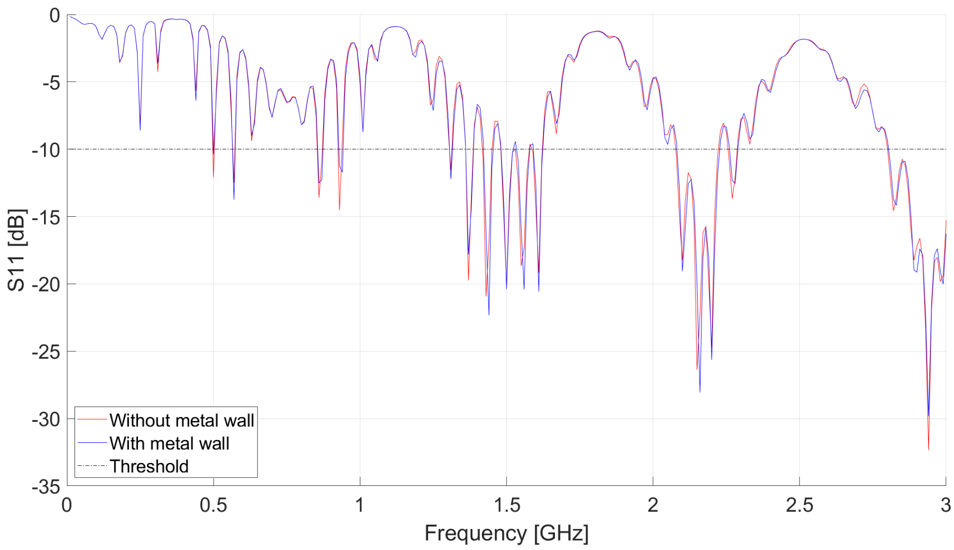

Figure 4.16: Overlaid S11 response of the Hilbert antenna inside the oil container without a metal wall (Red), with metallic wall (Blue).

4.1.2 Radiation pattern

To test the feasibility of using the HFA in oil-tanks for PD measurements, the antenna must be able to scan the entire region with equal gain around its boresight in order to detect PD occurrences no matter where they are generated, where the boresight can be defined as the axis with maximum gain, giving maximum radiated power for a directional antenna [24]. Thus, a study of the radiation pattern of the antenna would help in determining its efficacy. Figure 4.17 below shows the shape of the radiation pattern produced by the Hilbert antenna. The pattern is similar to a hemisphere with an gain around 0 dB around the boresight, where the gain decreases significantly the closer the look angle gets to 180° in any direction.

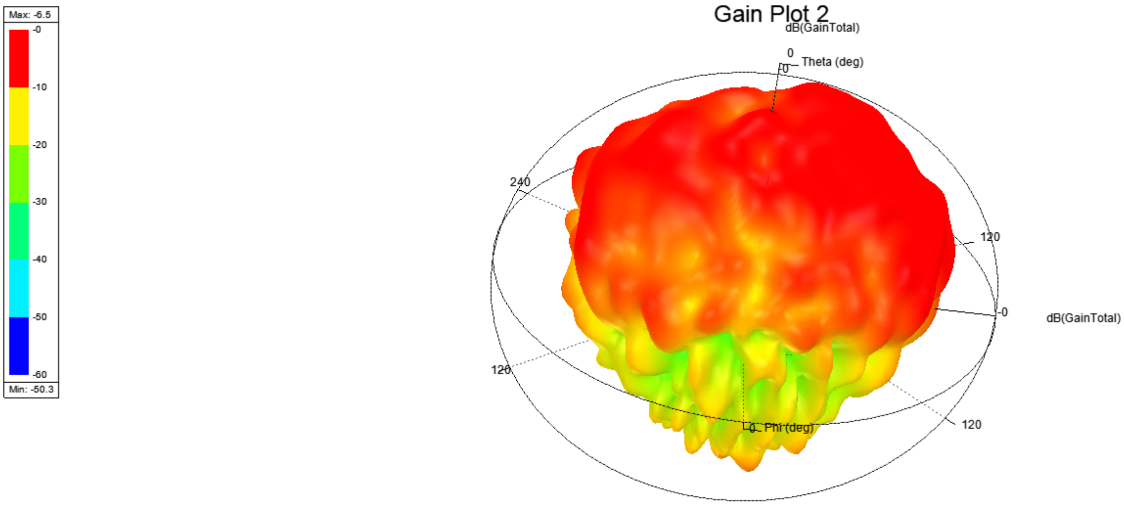

Figure 4.17: Simulated radiation pattern of the designed Hilbert antenna.

This proves that the HFA is suitable for this application and will be able to detect any PD activity allover the HV transformer. This is due to the radiation pattern shown above, which exhibits a typical patch antenna pattern that is mostly focused on one side of the patch and has a semi-stable gain around the boresight.

4.2 Correlation of PD Intensity Vs Captured Signal Energy

To understand how the Hilbert fractal antenna is capturing PD signals and then be able to calibrate it, correlation was made between the captured PD signals and the intensity levels given by the PD detector. To further illustrate, a quantitative value was extracted from the captured PD signal by computing the energy of the signal divided by the amplification factor. Then, the energy of each signal was plotted with its corresponding PD intensity value in **coulomb** C. A certain correlation was deduced from the scattered points on the graph depending on the value of the correlation coefficient R. The energy of the signal was computed using equation (4.2), and then scaled down to its original value before it was amplified with the LNA.

$$E_{PD} = \frac{\sum_{n=1}^{N} |x(n)|^2}{G_{LNA}} \tag{4.2}$$

where n is the index of the signal and it starts from 1 up to N, which is the total number of points in a signal. $x(n)$ is the sample PD signal. G_{LNA} is the linear gain of the amplifier which is equivalent to $10^{\frac{32}{10}}$.

Figures 4.18, 4.19 and 4.20 below are examples of twisted pair, sharp and void PD, respectively, in time domain. The capture PD signals display a typical transient shape where the signal starts abruptly and then shrinks down as if it follows an exponential curve. This transient trend confirms that the captured signals were indeed emitted from PD sources and follow the expected shape of a PD emission. The differences between the three types of PD samples below indicate that the signals contain different frequency components which would assist users in identifying the type of PD if the samples were passed through a classifier [10].

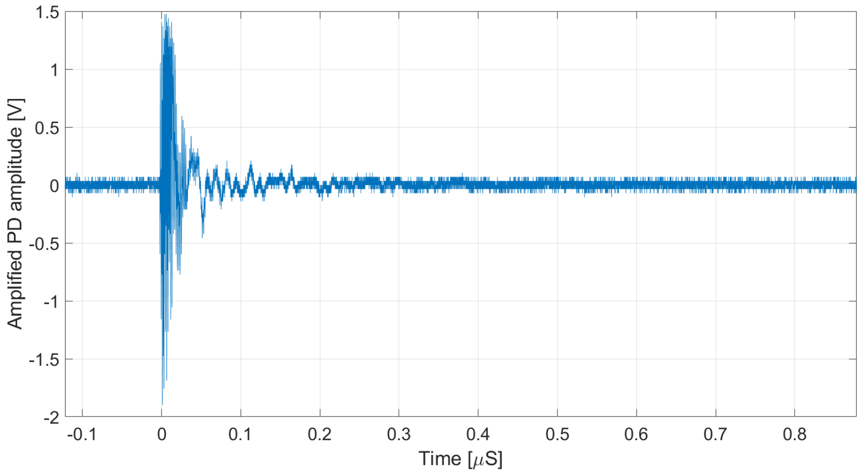

Figure 4.18: Sample twisted pair PD signal in time domain.

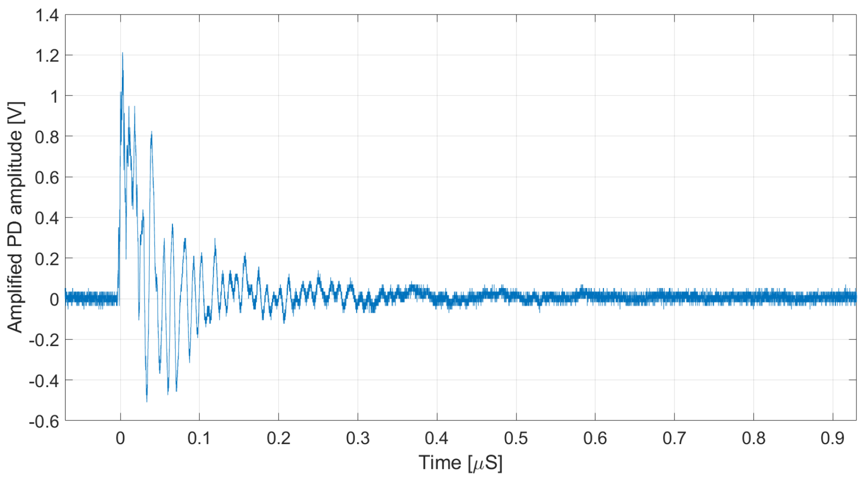

Figure 4.19: Sample sharp PD signal in time domain.

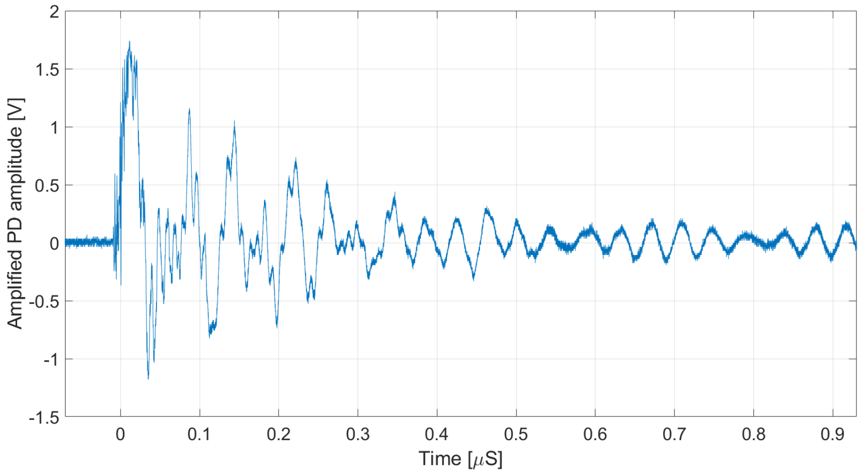

Figure 4.20: Sample void PD signal in time domain.

After computing the energy of around 50 samples per PD type, acquiring a quantitative measure of the captured signal, the energy was correlated with the PD intensity measured by the PD detector. This was done to find a calibration method for the antenna that would be standardized and approved. The correlation coefficient R was computed using equation (4.3)

$$R(A,B) = \frac{1}{N-1}\sum_{n=1}^{N}\frac{A_i-\mu_A}{\sigma_A}\frac{B_i-\mu_B}{\sigma_B} \tag{4.3}$$

where N represents the overall number of points for each random variable, A and B are the two random variables and μ_A and σ_A are the mean and the standard deviation of A, respectively, while μ_B and σ_B are the mean and the standard deviation of B, respectively.

4.2.1 Correlation in Air

Tests done outside the oil tank were collected and the energy of each sample of both PD types was correlated with its respective PD intensity level. In each of the following figures, the red line shows the computed trend of each scatter plot added to describe the approximated relationship of the samples.

Samples from the twisted pair PD were taken first, since the intensity of this type of PD can be varied. Figure 4.21 illustrates the correlation acquired from the collected samples. The relationship taken from the twisted pair PD shows a relatively weak positive correlation in air, with correlation coefficient $R =$ 0.354.

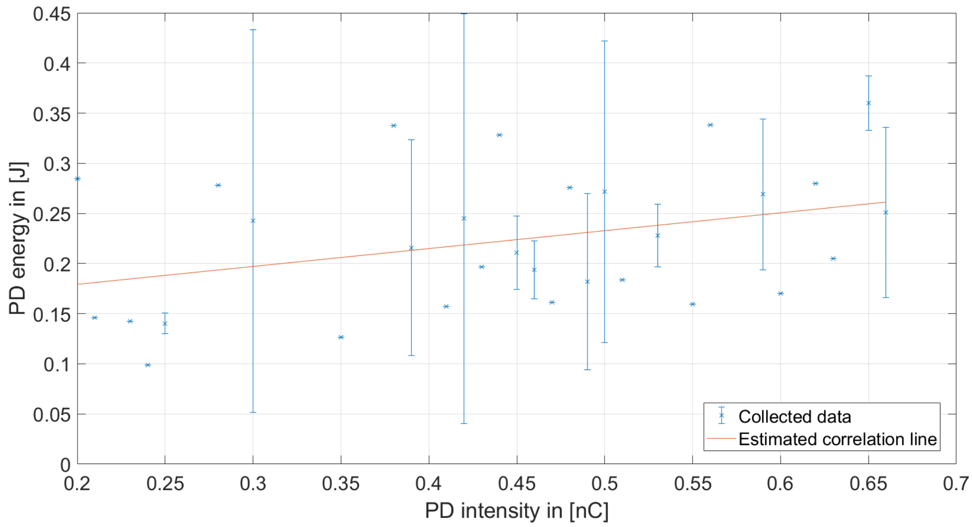

Figure 4.21: Analysis of twisted PD in air with PD intensity Vs signal energy level.

Figure 4.22 shows the distribution of points collected with the deviation of some of the repeated samples. An estimated correlation line was drown on the same figure where the correlation coefficient computed for this case was $R = 0.405$, which indicates a weak but positive correlation between the energy of the sharp PD in air and its corresponding PD intensity level.

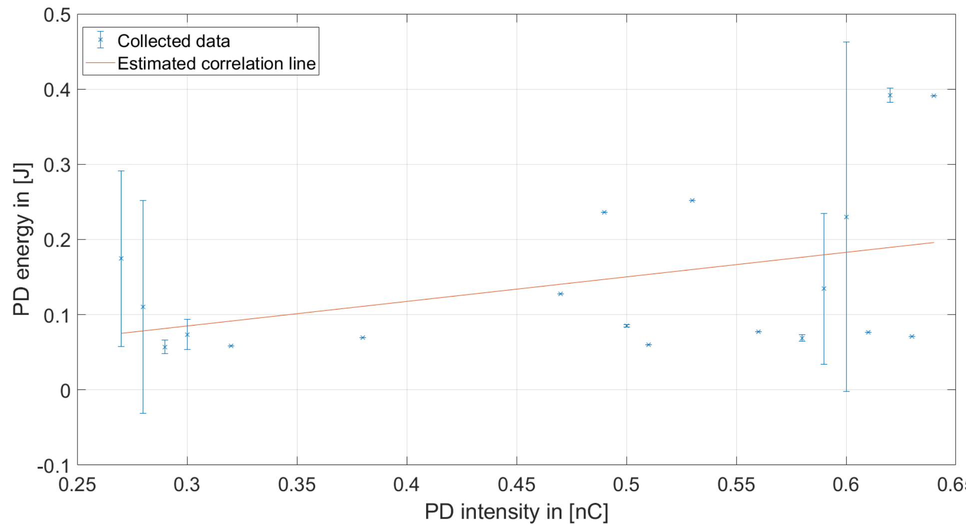

Figure 4.22: Analysis of sharp PD in air with PD intensity Vs signal energy level.

Void PD samples tested in air showed a similar trend, where points in figure 4.23 had a correlation coefficient $R = 0.492$ which is also a weak positive relationship. However, the values of both correlation coefficients for the different PD types are very close to each other showing that the experimental tests were consistent.

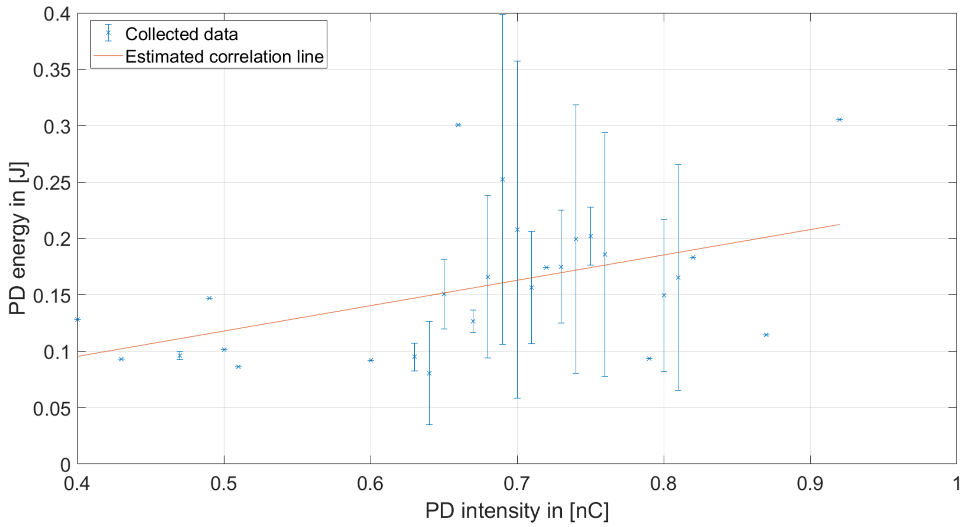

Figure 4.23: Analysis of void PD in air with PD intensity Vs signal energy level.

4.2.2 Correlation inside Oil

On the other hand, when the PD sources and Hilbert antenna were moved inside the oil tank, results changed and the values of the correlation coefficients changed accordingly. Starting with twisted pair PD in figure 4.24, the correlation coefficient $R =$ 0.701 indicating a relatively strong relationship between the capture PD intensity and the signal energy.

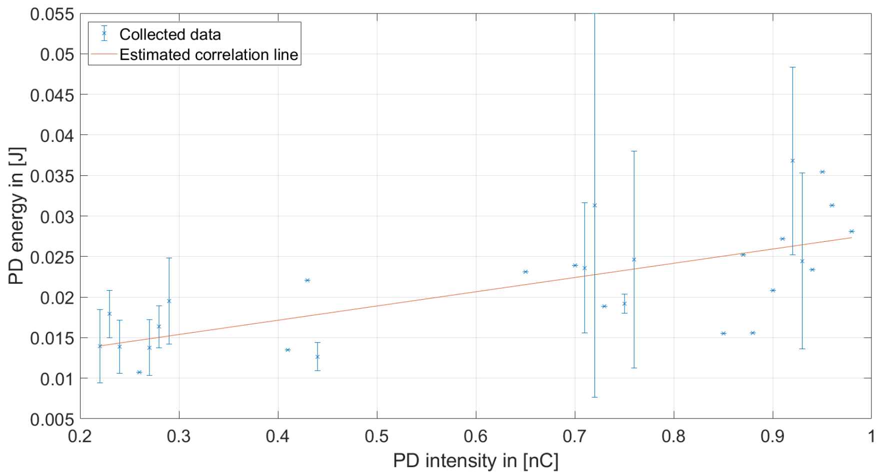

Figure 4.24: Analysis of twisted pair PD inside oil with PD intensity Vs signal energy level.

Figure 4.25 shows the trend obtained form the the sharp PD source when it was submerged in oil. The data points show a clear positive correlation with a correlation coefficient $R =$ 0.732, demonstrating a stronger correlation between the energy and the PD intensity.

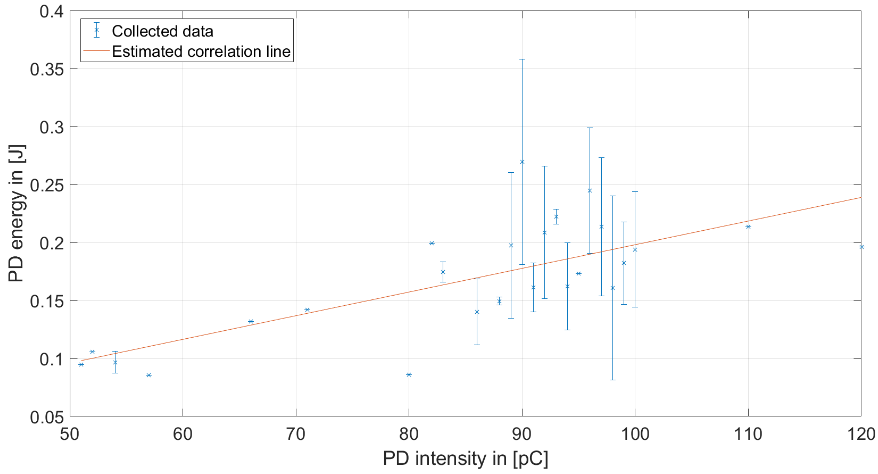

Figure 4.25: Analysis of sharp PD inside oil with PD intensity Vs signal energy level.

To confirm the results obtained from the twisted pair and sharp PD, figure 4.26 representing the void PD samples after submerging the source in oil shows the same positive correlation of points. The correlation coefficient of this test was $R = 0.825$ which is a stronger correlation than the one obtained from the twisted pair or sharp PD in oil. Having similar results for different PD sources depending on the environment they were placed at shows consistency of results and opens up room for discussion on effects of different mediums on the captured signals.

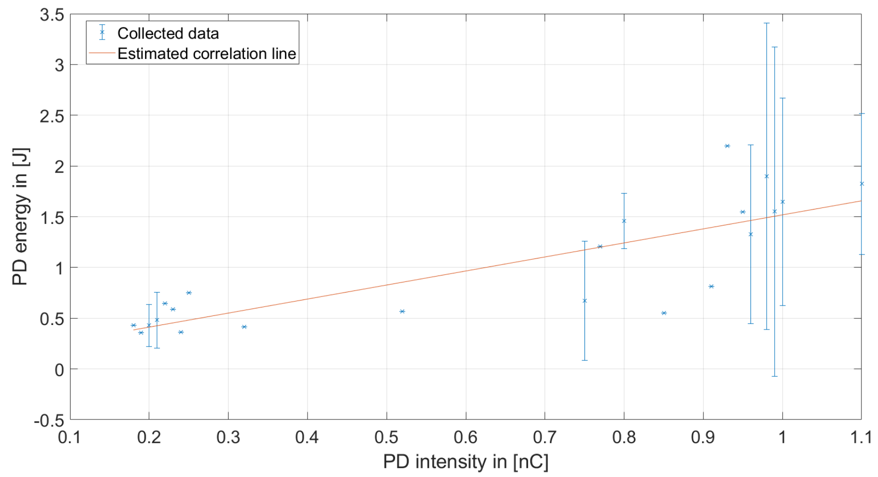

Figure 4.26: Analysis of void PD inside oil with PD intensity Vs signal energy level.

To summarize the relationships discussed for all PD types, table 4.4 shows the values for each test done. Tests in air showed low correlation coefficient and a weak positive relationship for all PD types, whereas tests done inside the oil-filled tank showed improved results and a stronger positive relationship. The reasons why this may have occurred and the implications of these results are discussed in the following section.

Table 4.4: Correlation coefficient of all PD types tested in air and inside oil

PD type	In air	Inside oil
Twisted pair	0.354	0.701
Sharp	0.405	0.732
Void	0.492	0.825

5

Discussion

Going back to the results acquired and starting with the designed 4^{th} order Hilbert antenna. The antenna showed wide coverage in the range of frequencies suggested for PD acquisition, from $300MHz$ to $3GHz$. The S11 parameter of the antenna was simulated and then tested in the lab, where it was shown that the coverage of the antenna in air covered around 28.7% of the frequency window. Moreover, when the antenna was submerged inside and oil-filled tank, the coverage increased to 31.3%. It is important to mention that the frequency response of the antenna experienced a non-linear frequency shift when submerged in oil, which was expected as the permittivity of the surrounding medium changed. Nonetheless, the aforementioned frequency shift did not affect the experiments conducted on the partial discharge sources, as the overall number of captured frequency components increased when the coverage increased. This was beneficial for the tests sinse it allowed more of the pulse‘s energy to be captured and digitized by the acquisition system. This was clearly shown in the section discussing the correlation of PD intensity with captured signal energy, where the correlation factor increased for all the tested sources giving a relatively stronger correlation between the two examined random variables.

Furthermore, to test the effects of metallic structures around the antenna and how they may change the frequency response, a metallic wall was placed around the test setup while examining the antenna. Results showed no side effects of the wall on the antenna response, indicating an effectively small far field range of the antenna. Meaning that, objects that are not closer than few centimeter from the antenna will not have any significant impact on the performance of the antenna.

The collected PD samples taken from the lab tests were supposed to be stable and consistent. However, results showed a varying uncertainty for each point of the random variable. This uncertainty was caused by several parameters, namely random PD activity, slow refresh rate of PD detector, varying amplifier temperature and human error. Each PD sources exhibited different performance when energized, the twisted pair PD was the most stable type of the sources tested, whereas the others showed significant PD intensity changes within short periods of time even when the applied voltage was fixed. The PD detector had a slow refresh rate of one reading per second, effectively slowing down the tests, especially when PD levels changed drastically, since the reading is an averaged value over time adding a transient effect on the displayed intensity level. Since the amplifier‘s internal temperature was not regulated, slight changes in the gain may have occurred which would affect the captured signal energy significantly. To overcome this temperature variation a temperature regulator must be applied to the amplifier in order to control the internal temperature. Human error also made an impact as the collected samples were synced with the displayed PD intensity level, and any delay or variation in the captured signal had an effect on the overall process. Finally, when the antenna was submerged inside the oil-filled tank, more voltage was applied to the PD sources to initiate the PD activity. This might have caused the PD signals to be more stable under higher electrical stress, which was showed in the improved results taken from the enhanced correlation.

6

Conclusion

Condition based maintenance focused on HV systems has become one of the attractions of the research industry. In particular finding an optimum and trust worthy method to detect insulation failure and classify operating systems based on their quality and durability level. Among many other methods of detection, the UHF antenna sensors are used to scan for anomalies within HV transformers, specifically looking for partial discharge activity as it is one of the main indicator of insulation breakdown. Thus, the Hilbert fractal antenna was designed, tested and manufactured to detect PD signals. However, that was not sufficient as the sensitivity of the sensor had to be tested and compared to a know detection system.

Thus, the focal point of this thesis project was to investigate the sensitivity of the Hilbert fractal antenna for the purpose of inspecting PD activity within HV transformers. To understand the antenna response in depth, it was tested with a vector network analyzer in different mediums, namely, in air, inside oil and covered with a conductive metallic wall. These different settings were chosen to monitor their effect on the resonant frequencies of the antenna as well as its overall performance. The data collected showed that the antenna is immune to the effects of conductive materials surrounding it and it performs better when submerged in oil.

The project utilized 3 different types of PD sources, namely: twisted pair, sharp point, and void. Each PD source was tested in air and inside an oil-filled tank. The collected data were correlated with their corresponding PD intensity level measured in nC. The relationship between the PD intensity and the detected signal energy was investigated for each type and a pattern was found. The relationship showed a weak positive correlation in air tests and a stronger positive correlation when placed inside oil.

The overall performance of the antenna was admirable as it had high sensitivity to PD activity of different types, in addition to resulting in consistent results under different conditions.

7

Future Work

Many other improvements can be done to further develop PD detection systems. In this thesis for example, further testing of the Hilbert fractal antenna must be done especially with a real power transformer. Testing the HFA along with a standard testing unit such as the apparent charge meter would allow better understanding of the response of the antenna in a real testing environments. In addition, allowing the antenna to work along side other PD sensors, such as the acoustic sensor or the high frequency current transformer, would help obtain better results as the different detection systems provide higher credibility to the occurrence of the PD phenomena and if tested and scaled to each other properly, the different detection systems might be able to work cooperatively.

Analyzing PD signals and measurement techniques is a lengthy process. It usually includes several PD sources, a sensor to capture PD activity and a proper data acquisition system. But what if the detection system used in the field detected different PD types, types that were not a part of the sources tested in the experimental stage, in this case the system might not respond as expected. A solution might be to implement a smart automated classification system that can be used to identify PD types detected and store their features and even if a new PD source appeared, the classification system would realize it does not belong to any of its already classified types and would train itself to classify it as an additional type which will be later stored in the detection system. By doing so, users would classify the captured PD signals in real time allowing for a more versatile approach to handling the issues as they occur.

Another variable to consider, especially in large power transformers, is the location of the PD source. Localizing PD sources within an enclosed environment is a field of its own. To localize PD sources at least 4 sensors of the same type must be used, those sensors must be calibrated to be as identical as possible in order to reduce any unwanted side effects that may occur due to variation in the response of the sensors. The location of each sensor must be studied depending on the dimensions of the power transformer, the type of the sensors, the operation range of the sensor, feasible placement points and other parameters that can be further investigated. By creating a system capable of localizing PD sources, users would be able to asses the situation better knowing both, the type and location of the PD source within a power transformer.

Bibliography

[1] P. Agoris, S. Meijer, and J. J. Smit. "Sensitivity Check of an Internal VHF/UHF Sensor for Transformer Partial Discharge Measurements". In: *2007 IEEE Lausanne Power Tech*. July 2007, pp. 2065–2069. DOI: 10.1109/PCT.2007.4538636.

[2] S. Coenen and S. Tenbohlen. "Location of PD sources in power transformers by UHF and acoustic measurements". In: *IEEE Transactions on Dielectrics and Electrical Insulation* 19.6 (Dec. 2012), pp. 1934–1940. ISSN: 1070-9878. DOI: 10.1109/TDEI.2012.6396950.

[3] S. Coenen et al. "Sensitivity of UHF PD measurements in power transformers". In: *IEEE Transactions on Dielectrics and Electrical Insulation* 15.6 (Dec. 2008), pp. 1553–1558. ISSN: 1070-9878. DOI: 10.1109/TDEI.2008.4712657.

[4] and D. Zhang. "Study on performance of HFCT and UHF sensors in partial discharge detection". In: *2010 Conference Proceedings IPEC*. Oct. 2010, pp. 630–635. DOI: 10.1109/IPECON.2010.5697070.

[5] B. Dong et al. "Sulfur Hexafluoride-Filled Extrinsic Fabry–PÉrot Interferometric Fiber-Optic Sensors for Partial Discharge Detection in Transformers". In: *IEEE Photonics Technology Letters* 20.18 (Sept. 2008), pp. 1566–1568. ISSN: 1041-1135. DOI: 10.1109/LPT.2008.928533.

[6] Tsutomu Endo et al. "Resonant frequency and radiation efficiency of meander line antennas". In: *Electronics and Communications in Japan (Part II: Electronics)* 83.1 (2000), pp. 52–58. DOI: 10.1002/(SICI)1520-6432(200001)83:1<52::AID-ECJB7>3.0.CO;2-7.

[7] J. Fuhr et al. *PARTIAL DISCHARGES IN TRANSFORMERS*. Tech. rep. CIGRE, Feb. 2017.

[8] B. Geng et al. "The comparison of sensitivity between the UHF and ultrasonic methods for partial discharge detecting in GIS". In: *2011 Annual Report Conference on Electrical Insulation and Dielectric Phenomena*. Oct. 2011, pp. 468–471. DOI: 10.1109/CEIDP.2011.6232696.

[9] D. W. Gross and M. Soller. "Partial discharge diagnosis on large power transformers". In: *Conference Record of the 2004 IEEE International Symposium on Electrical Insulation*. Sept. 2004, pp. 186–191. DOI: 10.1109/ELINSL.2004.1380511.

[10] M. M. O. Harbaji et al. "Design of Hilbert Fractal Antenna for Partial Discharge Classification in Oil-Paper Insulated System". In: *IEEE Sensors Journal* 17.4 (Feb. 2017), pp. 1037–1045. ISSN: 1530-437X. DOI: 10.1109/JSEN.2016.2638804.

[11] T. Hoshino et al. "Comparison of sensitivity between UHF method and IEC 60270 for onsite calibration in various GIS". In: *IEEE Transactions on Power Delivery* 21.4 (Oct. 2006), pp. 1948–1953. ISSN: 0885-8977. DOI: 10.1109/TPWRD.2006.874655.

[12] P. Kung et al. "Detection and location of PD activities using an array of fiber laser sensors". In: *2012 IEEE International Symposium on Electrical Insulation*. June 2012, pp. 511–515. DOI: 10.1109/ELINSL.2012.6251522.

[13] J. Li et al. "Optimization of UHF Hilbert Antenna for Partial Discharge Detection of Transformers". In: *IEEE Transactions on Antennas and Propagation* 60.5 (May 2012), pp. 2536–2540. ISSN: 0018-926X. DOI: 10.1109/TAP.2012.2189929.

[14] F. E. Lytle. *Impulse and Constant*. 2001. URL: https://www.chem.purdue.edu/courses/chm621/text/ft/basiset/impulse/impulse.htm.

[15] Gregor Pudlo. *Advanced PD Monitoring of Power Transformers Supporting Asset Management*. Website. 2007.

[16] M. Ren, M. Dong, and A. Qiu. "Partial discharges in SF6 gas filled void under standard aperiodic and oscillating switching impulses". In: *IEEE Transactions on Dielectrics and Electrical Insulation* 21.1 (Feb. 2014), pp. 262–272. ISSN: 1070-9878. DOI: 10.1109/TDEI.2013.004093.

[17] G. Robles et al. "Antenna Parametrization for the Detection of Partial Discharges". In: *IEEE Transactions on Instrumentation and Measurement* 62.5 (May 2013), pp. 932–941. ISSN: 0018-9456. DOI: 10.1109/TIM.2012.2223332.

[18] Y. Shaker, A. Zahed, and A. El-Hag. "Experience with acoustic sensors in partial discharge detection". In: *2016 IEEE International Conference on High Voltage Engineering and Application (ICHVE)*. Sept. 2016, pp. 1–4. DOI: 10.1109/ICHVE.2016.7800594.

[19] H. H. Sinaga, B. T. Phung, and T. R. Blackburn. "UHF sensor array for partial discharge location in transformers". In: *2012 IEEE International Conference on Condition Monitoring and Diagnosis*. Sept. 2012, pp. 979–982. DOI: 10.1109/CMD.2012.6416318.

[20] B. Song et al. "A New Optical Method of Partial Discharge Distant Positioning in GIS". In: *2018 IEEE Electrical Insulation Conference (EIC)*. June 2018, pp. 27–30. DOI: 10.1109/EIC.2018.8481103.

[21] *Technical Data sheet*. PE15A1007. Rev. 1.2. Pasternack Enterprises. 2016.

[22] K. J. Vinoy et al. "Resonant frequency of Hilbert curve fractal antennas". In: *IEEE Antennas and Propagation Society International Symposium. 2001 Digest. Held in conjunction with: USNC/URSI National Radio Science Meeting (Cat. No.01CH37229)*. Vol. 3. July 2001, 648–651 vol.3. DOI: 10.1109/APS.2001.960180.

[23] J. Volakis, C. Chen, and K. Fujimoto. *Small Antennas. Miniaturization Techniques Applications*. McGraw Hill Professional, 2009.

[24] Christian Wolff. *Radar Basics*. URL: http://www.radartutorial.eu/06.antennas/Monopulse%20Antenna.en.html.

[25] A. A. Zahed et al. "Comparison of different fourth order Hilbert fractal antennas for partial discharge measurement". In: *IEEE Transactions on Dielectrics and Electrical Insulation* 24.1 (Feb. 2017), pp. 175–182. ISSN: 1070-9878. DOI: 10.1109/TDEI.2016.005862.